Improving Ride Comfort Using Control Systems Design for Active Dampers

Master's thesis in Systems, Control and Mechatronics

Elham Goudarzi

Improving Ride Comfort Using Control Systems Design for Active Dampers

Elham Goudarzi

Department Mechanics and Maritime Sciences
Division of Vehicle Dynamics and Autonomous Systems
CHALMERS UNIVERSITY OF TECHNOLOGY
Gothenburg, Sweden 2019

Improving Ride Comfort Using Control Systems Design for Active Dampers

ELHAM GOUDARZI

Cover:

Improving Ride Comfort Using Control Systems Design for Active Dampers
Elham Goudarzi
Department of Mechanics and Maritime Sciences
Chalmers University of Technology

Abstract

There is a great demand for improvements in ride comfort of high-end passenger cars. Heave, roll and pitch motions might negatively affect ride comfort. In this regard, active and passive components are often integrated to improve vehicle dynamics performance. One of the challenges for automotive industry is to design controllers for active components used in the suspension system. The main focus here is to replace front and rear passive dampers with a set of active dampers integrated in parallel with coil springs within the suspension system. Such a setup can improve the overall performance of the vehicle by inducing or dispersing energy. Furthermore, it can reduce weight and energy consumption. However, such an active system might bring extra oscillation and disturbances to the vehicle. Hence, the integrated active dampers should be well controlled in order to operate as expected. The main objective of this study is to design a suitable control algorithm for the active dampers. A full vehicle model with 7 degrees of freedom (DOF) is validated in IPG CarMaker and used for the control design. Three different controllers are designed in Matlab: sky-hook controller, optimal controller with LQR method and robust controller with $\mathcal{H}_\infty$ method. The challenging part is tuning the parameters and weight selections for controllers. The controllers performances are verified and tested in IPG CarMaker and compared to the performance of a conventional passive suspension system. An overall improvement of the ride comfort is achieved in the simulations. It is recommended that the solutions are further assessed and developed in production vehicles and/or balancing with other performance indicators than comfort, such as handling and longitudinal performance.

Acknowledgements

Nomenclature

Abbreviations
DOF   Degree Of Freedom
LQR   Linear Quadratic Regulator
MPC   Model Predictive Control
LPV   Linear Parameter Varying
LTI   Linear Time Invariant
FFT   Fast Fourier Transform
RMS   Root Mean Square

x

x

Contents

1
Introduction

To improve ride comfort in passenger cars, mitigating vibrations induced by road roughness is essential. There are several factors that can affect ride comfort, such as roll, pitch and heave oscillations [1], [2], [3]. Passive dampers, anti-roll bars, semi-active dampers [4], [5] are widely used to improve vehicle performance from different points of view. Introducing the new technology of active damper suspension makes it possible to replace passive dampers while achieving a suitable level of ride comfort. These active actuators have to cope with roll, pitch and heave disturbances. Such components can theoretically smoothen the driving experience by reducing vertical acceleration, roll acceleration and pitch acceleration. However, control design for such components is an elaborate task. To ensure active dampers run stable and reliable, it is essential to design a suitable control algorithm, which is the main goal of this study.

1.1 Background

There are several suspension system components that can positively influence ride comfort. On a passive vehicle suspension, they are mainly springs, anti-roll bars and shock absorbers, also known as dampers. Let us now assume to replace the passive dampers with by active dampers. Active suspension actuators cover a wider range of maximum and minimum force limits compared to semi-active dampers; therefore active dampers have a higher potential impact on ride comfort. Active dampers can stabilize in 3 degrees of freedom of the car body heave, roll and pitch considering that they have less constraints; hence, active anti-roll bars is removed in the full car model by adding active dampers. The task of the active actuators is to balance the extra forces induced to the vehicle body to improve suspension performance. Active actuator together with a suitable controller improves ride comfort. Thus from capability and performance perspective, active suspensions are often preferred to passive design. This thesis aims to improve active suspension system with development of a suitable control algorithm and active dampers. For ride comfort improvement, robust control such as $\mathcal{H}_\infty$ and LPV $\mathcal{H}_\infty$ [6], optimal control method such as LQR [7] and MPC with road preview [8] have been investigated. As an example, active components such as semi-active dampers and active anti-roll bars are integrated to passenger cars by applying LQR with control allocation, $\mathcal{H}_\infty$ with control allocation and LPV-$\mathcal{H}_\infty$ [6]. $\mathcal{H}_\infty$ controllers for quarter car model, half car model and full car model have been investigated[9]. It should be stated that nothing found in public report for the controller choice of a production car with active suspension

1.2 Objective

The objective of this thesis is to design and analyze different control strategies, including sky-hook, optimal control with LQR and robust control with $\mathcal{H}_\infty$. The objective is to improve ride comfort of a car with active suspension system by controlling the active dampers.

1.3 Deliverables

Contributions of this thesis include:

1. Modelling the 7DOF full car model with active dampers
2. Investigation and development of 3 controllers for the active dampers and testing on standard scenarios for ride analysis
3. Ride comfort improvement by controlling active dampers within the vehicle suspension system

The full car model is simulated in MATLAB to model the vibration dynamics of a vehicle. Several control methods are developed and tested in IPG CarMaker [10] which is a nonlinear simulation environment. The controllers are studied to improve the ride comfort.

1.4 Limitations

In this thesis, controllers for the active suspensions are implemented with MATLAB and IPG CarMaker. In controller designs, the motion effect in ground plane via tire to road grip has been neglected and road grip has been limited for handling, braking and traction. Also it is assumed that all the state measurements are available at a time and states do not have time delay or limitation. It should be noted that the influence on handling target and longitudinal motion performance is not studied in this thesis.

1.5 Thesis Outline

The thesis starts at chapter 2 with control methodologies studies for all three controllers. The theories behind the controllers including sky-hook control, LQR control and $\mathcal{H}_\infty$ control are described.

Next, in chapter 3 an overview of vehicle dynamics and actuator model is presented. The vehicle dynamics section starts with the description of the quarter car model; then the full car model is presented. Also, the relation between full car model and actuators is presented and the state space representation is defined. Different types of actuators used in the suspension system are described.

In chapter 4, the method of controller evaluation is described. Then the controller implementation of all three controllers is presented separately. The selection of weighting factors methods for tuning the controllers are explained. Control system overviews of LQR and $\mathcal{H}_\infty$ are shown in section 4.2.3 and 4.2.5, respectively. Finally,

the verification of MATLAB analytical model is carried out for accuracy confirmation.

The control implementation results are presented in chapter 5. Four different test cases are used to test the controller performance and to discuss the results.

In chapter 6, all the work from previous chapters is discussed and recommendations for future work and further development are proposed.

Finally, Chapter 7 reports the thesis conclusion to summarize the research activity.

2
Control Methodologies Theory

In this chapter, the control methods used in the thesis are described. Active control consists of optimal control strategy and robust control strategy. Semi-active control consists of sky-hook control strategy.

2.1 Sky-hook control

Semi-Active vibration control is a control system that adjusts the forces applied by active dampers. In this way, the forces on the suspension system are changed as a function of time. Active damper forces can be controlled in real-time optimally, the suspension system performance can be improved. The semi-active control strategy based on sky-hook approach is presented [11].

The height variation of the road profile and of the unsprung masses are measured and fed into the sky-hook controller.Variables $\dot{x}(t)$ and $\dot{y}(t)$, are the absolute velocities of sprung mass and unsprung mass respectively. The controller tunes the actuator forces such that the force, which is proportional to the relative velocity $\dot{x}(t) - \dot{y}(t)$ between road and unsprung mass, can be varied as a function of time.

2.1.1 Continuous Sky-hook Strategy

Consider a vibrating system featuring a sky-hook damper where c_{sk} is the damping coefficient and $\dot{x}(t)$ is the absolute vertical velocity of the oscillating mass. Damping force formula follows [11]:

$$F_{sk} = c_{sk}\dot{x}(t) \tag{2.1}$$

The objective is to replicate the damping force F_{sk} of a semi-active damper between the base and the mass [11]:

$$F_{sa} = \begin{cases} c_{sk}\dot{x}(t); & \dot{x}(t)(\dot{x}(t) - \dot{y}(t)) \geq 0 \\ 0; & \dot{x}(t)(\dot{x}(t) - \dot{y}(t)) < 0 \end{cases} \tag{2.2}$$

When the semi-active damper is off, $\dot{x}(t)$ and $\dot{x}(t) - \dot{y}(t)$ are opposite in sign and so damping force is zero. On the other hand, when the semi-active damper is on, the damping force F_{sa} can be written as [11]:

$$F_{sa} = c_{sa}(\dot{x}(t) - \dot{y}(t)) \tag{2.3}$$

c_{sa} is semi-active damping coefficient. By inserting above equation c_{sa} will be as follows [11]:

$$c_{sa} = \begin{cases} c_{sk} \frac{\dot{x}(t)}{\dot{x}(t)-\dot{y}(t)} & \dot{x}(t)(\dot{x}(t)-\dot{y}(t)) \geq 0 \\ c_{min} & \dot{x}(t)(\dot{x}(t)-\dot{y}(t)) < 0 \end{cases} \tag{2.4}$$

c_{sa} has lower bound of minimum damping coefficient and upper bound of maximum damping coefficient. Finally, the damping coefficient can be written as [11]:

$$c_{sa} = \begin{cases} min[c_{sk} \frac{\dot{x}(t)}{\dot{x}(t)-\dot{y}(t)}, c_{max}] & \dot{x}(t)(\dot{x}(t)-\dot{y}(t)) \geq 0 \\ c_{min} & \dot{x}(t)(\dot{x}(t)-\dot{y}(t)) < 0 \end{cases} \tag{2.5}$$

2.1.2 On-off Sky-hook Strategy

The on-off sky-hook strategy can be used to simplify the control process comparing to continuous one. The on-off semi-active damper acts as conventional passive damper with the maximum damping coefficient c_{max} during the vibration phase and minimum damping coefficient when in opposite direction to the ideal sky-hook damping force [11].

$$c_{sa} = \begin{cases} c_{max} & \dot{x}(t)(\dot{x}(t)-\dot{y}(t)) \geq 0 \\ c_{min} & \dot{x}(t)(\dot{x}(t)-\dot{y}(t)) < 0 \end{cases} \tag{2.6}$$

The semi-active controller acts as a conventional passive controller by applying the maximum force F_{max} when the damping is needed, but a minimum force F_{min} is assumed when the force generated by actuator would be in the opposite direction compared to the ideal sky-hook force. The semi-active force on on-off sky-hook strategy is then:

$$F_{sa} = \begin{cases} c_{max}(\dot{x}(t)-\dot{y}(t)) & \dot{x}(t)(\dot{x}(t)-\dot{y}(t)) \geq 0 \\ c_{min}(\dot{x}(t)-\dot{y}(t)) & \dot{x}(t)(\dot{x}(t)-\dot{y}(t)) < 0 \end{cases} \tag{2.7}$$

The maximum force, which is the on-state force, is much greater than the minimum force of the off-state.

2.2 Optimal Control Strategy

The optimal control aims to find a control law that fulfills a predefined optimal criterion for a given system. One of the control strategies in optimal control method is linear quadratic regulator, which is a feedback controller.

2.2.1 Linear Quadratic Regulator

Linear quadratic regulator is an alternative to select closed loop eigenvalues location which enables closed loop stability and high performance of system. LQR is one of the most commonly used optimal control problems. The gain for state feedback controller to accomplish a certain objective can be chosen by optimizing a cost function .

Consider a multi-input linear system [12]:

$$\dot{x}(t) = Ax(t) + Bu(t) \qquad x \in \mathbb{R}^n, u \in \mathbb{R}^p \tag{2.8}$$

The assumption is that all the system states are available for measurement and the system states are available for controlling.
The optimal control law is given by [12]:

$$\begin{aligned} u(t) &= -\bar{K}x(t) \\ \bar{K} &= R^{-1}B^T\bar{P} \end{aligned} \tag{2.9}$$

A cost function is a performance equation which describes the system behaviour and evaluates how well the algorithm performs the optimization problem. LQR attempts to minimize the cost function [12]:

$$\begin{aligned} \min_{u(t)} J &= \min_{u(t)} \frac{1}{2} \int_0^\infty (x^T(t)Qx(t) + u^T(t)Ru(t))dt \\ &= \min_{u(t)} \frac{1}{2} \left\| Q^{\frac{1}{2}}x(t) \right\|_2^2 + \frac{1}{2} \left\| R^{\frac{1}{2}}u(t) \right\|_2^2 \end{aligned} \tag{2.10}$$

K is the state feedback gain matrix and it is subjected to minimize J as cost function.
Where $Q \geq 0$ is a symmetric and positive semi definite matrix and $R > 0$ is a symmetric and positive definite matrix.
$\bar{P}$ matrix in equation 2.9 is the solution to the LQR as [12]:

$$A^T\bar{P} + \bar{P}A + \bar{P}BR^{-1}B^T\bar{P} = 0 \tag{2.11}$$

LQR has the ability to find a trade-off between states errors and control efforts through Q and R. This will give the opportunity to prioritize those states that are critical to minimize their deviations. Also, limitations of control inputs can be considered.
To select weighting factors matrices, the largest desired state response $x_{i,max}$ and the largest desired control inputs $u_{i,max}$ are used to normalize weights. Relative weights on states and inputs are used to find better set of weightings:

$$Q = \begin{bmatrix} \frac{\alpha_1^2}{x_{1,max}^2} & 0 & \cdots & 0 \\ 0 & \frac{\alpha_2^2}{x_{2,max}^2} & \cdots & 0 \\ \cdots & \cdots & \ddots & \cdots \\ 0 & 0 & \cdots & \frac{\alpha_n^2}{x_{n,max}^2} \end{bmatrix} \tag{2.12}$$

$$R = \begin{bmatrix} \frac{\beta_1^2}{u_{1,max}^2} & 0 & \cdots & 0 \\ 0 & \frac{\beta_2^2}{u_{2,max}^2} & \cdots & 0 \\ \cdots & \cdots & \ddots & \cdots \\ 0 & 0 & \cdots & \frac{\beta_n^2}{u_{n,max}^2} \end{bmatrix} \tag{2.13}$$

2.2.2 State Derivatives Penalization in a Cost Function

To improve ride comfort, our aim is to minimize the roll, pitch and heave accelerations. Heave rate, roll rate and pitch rate are available as states so they can be penalized through the weighting matrices. $\ddot{z}$, $\ddot{\theta}$ and $\ddot{\phi}$ are not included in the state vector, but LQR can be extended to penalize them in the control problem.
To control state derivatives, $\dot{x}(t)$, a new cost function can be defined as [13]:

$$J = \frac{1}{2} \int_0^\infty (\dot{x}(t)Q_1\dot{x}(t) + x(t)Q_2x(t) + u^T(t)Ru(t))dt \tag{2.14}$$

Q_1 and Q_2 are weight matrices. Substituting the state space into the cost function gives [13]:

$$J = \frac{1}{2} \int_0^\infty ((Ax(t) + Bu(t))^T Q_1(Ax(t) + Bu(t)) + (x^T(t)Q_2x(t) + u^T(t)Ru(t))dt$$
$$= \frac{1}{2} \int_0^\infty (x^T(t)A^T + u^T(t)B^T)Q_1(Ax(t) + Q_1Bu(t)) + u^T(t)Ru(t) + x^T(t)Q_2x(t))dt$$
$$= \frac{1}{2} \int_0^\infty (x^T(t)\tilde{Q}x(t) + x^T(t)\tilde{N}u(t) + u^T(t)\tilde{N}x(t) + u^T(t)\tilde{R}u(t))dt \tag{2.15}$$

Where $\tilde{Q} = (A^TQ_1A + Q_2)$, $\tilde{R} = (B^TQ_1B + R)$ and $\tilde{N} = A^TQ_1B$

2.3 Robust Control Strategy

Although sky-hook control and LQR control achieve a good tracking and reasonable response, when there are uncertainties and disturbances in industrial systems, these control systems cannot guarantee stability. In this regard, robust control strategy can be used to design a more suitable control system. A control system is robust if it remains stable and keep certain performance criteria in presence of possible uncertainties. Robust control strategy is used to design a controller for a system such

that the closed-loop system is stable. Robust control systems are tolerant to system changes and perturbations such as disturbances and uncertainties [14]. It has the possibility to include frequency dependent weights that considers the limitation on multiple actuators in the system.

Robustness has always been a critical issue regarding the design of the control systems. Robustness is about the control system ability to deal with uncertainties of system dynamics or environment conditions, and to maintain stability and performance. Robust control is a new method in control theory which has been developed throughout the recent years. There are different robust control methods such as $\mathcal{H}_2$, $\mathcal{H}_\infty$, mixed sensitivity $\mathcal{H}_\infty$ and μ synthesis.

2.3.1 $\mathcal{H}_\infty$ Description

There is a generalized plant P (with two groups of inputs and two groups of outputs) and a controller K. The plant has w, weighted exogenous inputs including reference signals and disturbances, and u, control signals, as inputs. The outputs are z, weighted exogenous outputs, error signals which we want to minimize. y sensed outputs are measured to be controlled [15]. The control structure is shown in figure 2.1
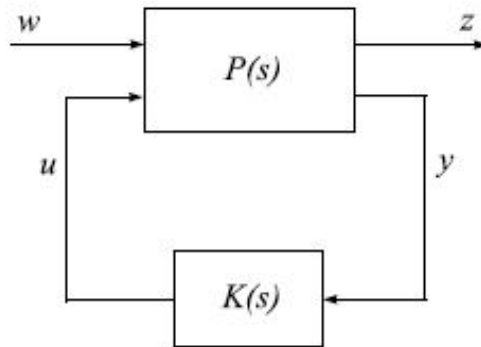
Figure 2.1: $\mathcal{H}_\infty$ control structure [15]

The objective is to minimize a $\mathcal{H}_\infty$ norm of output errors with input disturbances while finding a controller K with internal closed loop stability.

2.3.2 $\mathcal{H}_\infty$ System Norm

The $\mathcal{H}_\infty$ norm is the peak value of the transfer function plot. Considering a transfer function $G(s)$ with $U(s)$ as input and $Y(s)$ as output in frequency domain, the H_∞ norm is [14] :

$$\|G(s)\|_\infty = \max_\omega \bar{\sigma}(G(i\omega)) \tag{2.16}$$

H_∞ norm is interpreted as a peak to peak amplification. The H_∞ norm is the peak

of induced 2 norm as well. Definition of H_∞ norm in time domain is[14] :

$$\|G(s)\|_\infty = \max_{u(t) \neq 0} \frac{\|y(t)\|_2}{\|u(t)\|_2} = \max_{\|u(t)\|_2 = 1} \|y(t)\|_2 \tag{2.17}$$

$G(i\omega)$ frequency is bounded between 2 singular values where [14]:

$$\underline{\sigma}(G(i\omega)) \leq \frac{\|y(i\omega)\|_2}{\|u(i\omega)\|_2} \leq \bar{\sigma}(G(i\omega)) \tag{2.18}$$

The peak of the largest singular value of ω plot makes a norm.

2.3.3 Robust Stabilization

For $\mathcal{H}_\infty$ optimization problems, Small-Gain Theorem is sufficient and necessary for system stability. Consider the two interconnected systems in figure 2.2, where $G_1(s)$ and $G_2(s)$ are transfer functions for LTI systems [15]:
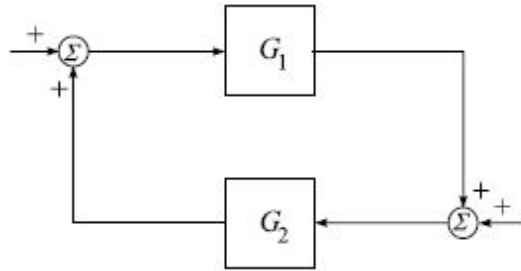
Figure 2.2: Interconnected systems in feedback configuration [15]

Theorem 2.1 *If $G_1(s)$ and $G_2(s)$ are stable, i.e. $G_1 \in \mathcal{H}_\infty, G_2 \in \mathcal{H}_\infty$, then the closed loop system is internally stable if and only if*[15]

$$\|G_1 G_2\|_\infty < 1 \quad and \quad \|G_2 G_1\|_\infty < 1 \tag{2.19}$$

A closed loop system of the plant G and controller K has robust stability if it holds stability for all possible perturbations on the system plant. So K is a stabilizing controller for the plant. The perturbation set is assumed to be zero. In this regards, an input multiplicative perturbation, shown in figure 2.3, $\Delta(s)$, is considered, where $\Delta(s)$ is an unknown matrix. The transfer function from u to v is $G_{uv} = -K(I + GK)^{-1}$. [15]
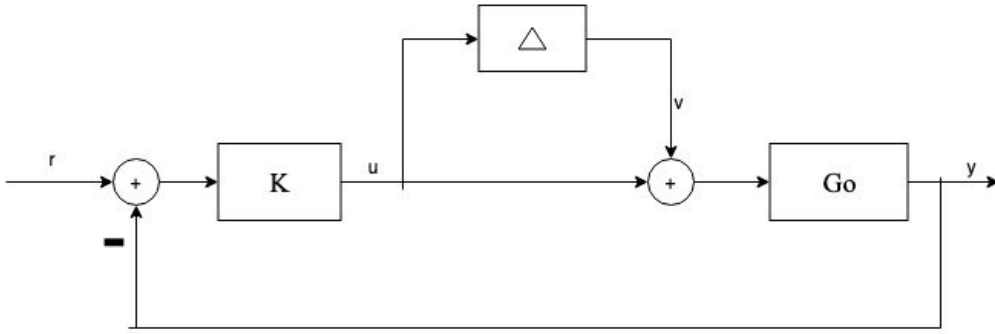
Figure 2.3: Interconnected systems in feedback configuration [15]

Theorem 2.2 *For a stable $\Delta(s)$, the closed loop system has robust stability if $K(s)$ stabilizes the nominal plant and the following holds:* [15]

$$\left\| KG(I + GK)^{-1} \right\|_{\infty} < \frac{1}{\|\Delta\|_{\infty}} \tag{2.20}$$

For $\infty - norm$ it is required to find a controller that has robust stability for all the possible set of perturbations.

$$\min_{K stabilizing} \left\| KG(I + GK)^{-1} \right\|_{\infty} \tag{2.21}$$

If the perturbation is such that $\bar{\sigma}(\Delta(j\omega)) \leq \bar{\sigma}(W_2(j\omega))$ for all $\omega \in R$, then the perturbation block is written as $\Delta(s) = \tilde{\Delta}(s)W_2(s)$. $\tilde{\Delta}(s)$ is the unit norm perturbation set. Hence, the robust stabilization and optimization problem becomes[15]:

$$\left\| W_2 KG(I + GK)^{-1} \right\|_{\infty} < 1 \tag{2.22}$$

$$\min_{K stabilizing} \left\| W_2 KG(I + GK)^{-1} \right\|_{\infty} \tag{2.23}$$

Robust stabilization is required to formulate the stability and to solve the robust optimization problem.

2.3.4   Performance

Figure 2.3 illustrates a typical closed loop control system, where G is the plant and K is the controller. r, y, u, e, d, and n are reference, input, output, control signal, error signal , disturbance and measurement noise, respectively .

For performance specifications, it should be noted that the signals r, d and n are energy bounded and do not exceed 1.

Base on system norms, the ∞ norm of transfer function matrices should be minimized. So the performance problem is to find an optimal solution out the set of stabilizing controllers K, for a certain performance specifications. Performance

specifications are listed as below:

1. Tracking

$$\|(I + GK)^{-1}\|_\infty \tag{2.24}$$

2. Disturbance attenuation

$$\|(I + GK)^{-1}\|_\infty \tag{2.25}$$

3. Noise rejection

$$\|-(I + GK)^{-1}GK\|_\infty \tag{2.26}$$

4. Less control energy

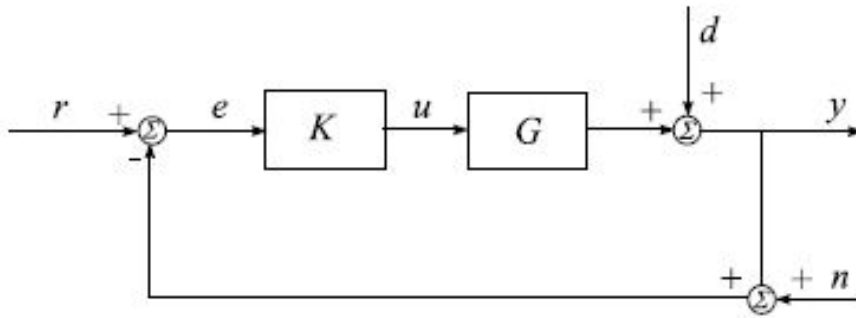$$\left\|K(I + GK)^{-1}\right\|_\infty \tag{2.27}$$

Figure 2.4: Closed loop control system [15]

2.3.5 $\mathcal{H}_\infty$ Control Method

The state space description of the generalized system P in figure 2.1 is given by [14]:

$$\begin{aligned}
\dot{x}(t) &= Ax(t) + B_1\omega(t) + B_2u(t) \\
z(t) &= C_1x(t) + D_{11}\omega(t) + D_{12}u(t) \\
y(t) &= C_2x(t) + D_{21}\omega(t)
\end{aligned} \tag{2.28}$$

The control problem is equivalent to minimizing the $\mathcal{H}_\infty$ norm of the transfer function from ω to z. Let us partition the interconnected system P as

$$P = \begin{bmatrix} P_{11} & P_{12} \\ P_{21} & P_{22} \end{bmatrix} = \left[\begin{array}{c|cc} A & B_1 & B_2 \\ \hline C_1 & D_{11} & D_{12} \\ C_2 & D_{21} & D_{22} \end{array} \right] \tag{2.29}$$

The system and the stabilizing controller K are described as:

$$\begin{bmatrix} \dot{x} \\ z \\ v \end{bmatrix} = P \begin{bmatrix} x \\ \omega \\ u \end{bmatrix} \tag{2.30}$$

$$u = Kv \tag{2.31}$$

Where $x \in \mathbb{R}^n, u \in R^m, \omega \in R^q$ and $z \in R^r$.
Hence the control problem is formulated as state feedback structure with closed loop lower linear fractional transformation of P and K [14]:

$$z = \mathcal{F}_1(P, K)\omega \tag{2.32}$$

Where

$$\mathcal{F}_l(P, K) = P_{11} + P_{12}K(I - P_{22}K)^{-1}P_{21} \tag{2.33}$$

The design objective, which is referred as the $\mathcal{H}_\infty$ optimization problem, becomes:

$$\min_{K\,stabilizing} \|\mathcal{F}_1(P, K)_\infty\| \tag{2.34}$$

2.3.6 $\mathcal{H}_\infty$ Suboptimal Problem

In practical design of $\mathcal{H}_\infty$ control, it is usual to solve the problem by finding a stabilizing controller K such that $\|\mathcal{F}_1(P, K)_\infty\| < \gamma$, where γ is positive and $\gamma > \gamma_0 := \min_{K\,stabilizing} \|\mathcal{F}_1(P, K)_\infty\|$ [15]. This is the $\mathcal{H}_\infty$ Suboptimal Problem.
Consider the state space description in (2.8) where P a partitioned interconnected system as:

$$P = \left[\begin{array}{c|c} A & B \\ \hline C & D \end{array} \right] \tag{2.35}$$

It is assumed that there is no relation between the control input and the measurement output, $D_{22} = 0$. This is a reasonable assumption, due to the fact that majority of industrial control systems are strictly proper systems and the D_{22} of the plants has zero values. The $\mathcal{H}_\infty$ solution formulas use set of solutions of two algebraic Riccati equations (ARE). Consider an algebraic Riccati equation [15]:

$$E_T X + XE - XWX + Q = 0 \tag{2.36}$$

where $W = W^T$ and $Q = Q^T$ corresponds to a Hamilton matrix

$$\begin{bmatrix} E & -W \\ Q & -E_T \end{bmatrix} \tag{2.37}$$

The X solution of the ARE is the stabilizing solution and is a symmetric matrix. In this case, $E - WX$ is a stable matrix. The stabilizing solution is

$$X := \mathbf{Ric} \begin{bmatrix} E & -W \\ Q & -E_T \end{bmatrix} \tag{2.38}$$

Define

$$R_n := D_{1*}^T D_{1*} - \begin{bmatrix} \gamma^2 I_{m1} & 0 \\ 0 & 0 \end{bmatrix}$$
$$\tilde{R}_n := D_{1*} D_{1*}^T - \begin{bmatrix} \gamma^2 I_{p1} & 0 \\ 0 & 0 \end{bmatrix} \tag{2.39}$$

where $D_{1*} =$
$\begin{bmatrix} D_{11} & D_{12} \end{bmatrix}$ and $D_{1*} = \begin{bmatrix} D_{11} \\ D_{21} \end{bmatrix}$. We assume that R_n and $\tilde{R}_n$ are non singular. We define two Hamiltonian matrices H and J as

$$\mathbf{H} := \begin{bmatrix} A & 0 \\ -C_1^T C_1 & -A^T \end{bmatrix} - \begin{bmatrix} B \\ -C_1^T D_{1*} \end{bmatrix} R_n^{-1} \begin{bmatrix} D_{1*}^T C_1 & B^T \end{bmatrix} \tag{2.40}$$

$$\mathbf{J} := \begin{bmatrix} A_T & 0 \\ -B_1 B_1^T & -A \end{bmatrix} - \begin{bmatrix} C^T \\ -B_1 D_{1*}^T \end{bmatrix} \tilde{R}_n^{-1} \begin{bmatrix} D_{1*} B_1^T & C \end{bmatrix} \tag{2.41}$$

Let

$$X := \mathbf{Ric}(\mathbf{H})$$
$$Y := \mathbf{Ric}(\mathbf{J}) \tag{2.42}$$

Regarding X and Y, there are a state feedback matrix F and an observer gain matrix L, which will be used in the following solution formulas [15],

$$F := -R_n^{-1}(D_{1*}^T C_1 + B_T X) =: \begin{bmatrix} F_1 \\ F_2 \end{bmatrix} =: \begin{bmatrix} F_{11} \\ F_{12} \\ F_2 \end{bmatrix} \tag{2.43}$$

$$L := (B_1 D_{*1}^T + Y C_T) - \tilde{R}_n^{-1} =: \begin{bmatrix} L_1 & L_2 \end{bmatrix} =: \begin{bmatrix} L_{11} & L_{12} & L_2 \end{bmatrix} \tag{2.44}$$

where F_1, F_2, F_{11} and F_{12} have m_1, m_2, $m_1 - p_2$ and p_2 rows, respectively, and L_1, L_2, L_{11} and L_{12} have p_1, p_2, $p_1 - m_2$ and m_2 columns, respectively.
Glover and Doyle [13] derived a $\mathcal{H}_\infty$ suboptimal solution which is necessary and sufficient. The solution is obtained based on following assumptions:

1. (C_2, A) is detectable and (A, B_2) is stabilizable;

2. $D_{12} = \begin{bmatrix} 0 \\ I_{m2} \end{bmatrix}$ and $D_{21} = \begin{bmatrix} 0 & I_{p2} \end{bmatrix}$;

3. $\begin{bmatrix} A - j\omega I & B_2 \\ C_1 & D_{12} \end{bmatrix}$ has full column rank for all ω;

4. $\begin{bmatrix} A - j\omega I & B_2 \\ C_2 & D_{21} \end{bmatrix}$ has full row rank for all ω.

Together with partition of

$$D_{11} = \begin{bmatrix} D_{1111} & D_{1112} \\ D_{1121} & D_{1122} \end{bmatrix} \tag{2.45}$$

where D_{1122} has m_2 rows and p_2 columns [15].

2.3.7 The Selection of Weighing Factors

$\mathcal{H}_\infty$ control has the ability to include frequency dependent weights. These weighting factors are designed to penalize control effort and error, disturbance and noises.

In this control structure there are four weighting factors to design, which are shown in figure 2.5. W_u is needed to include the dynamics of a band width limited actuator and to restrict the control effort signal. W_e is needed to penalize certain states and it affects the system performance. W_n and W_d are the upper bounds for measurement noise and input disturbance [16] [17].
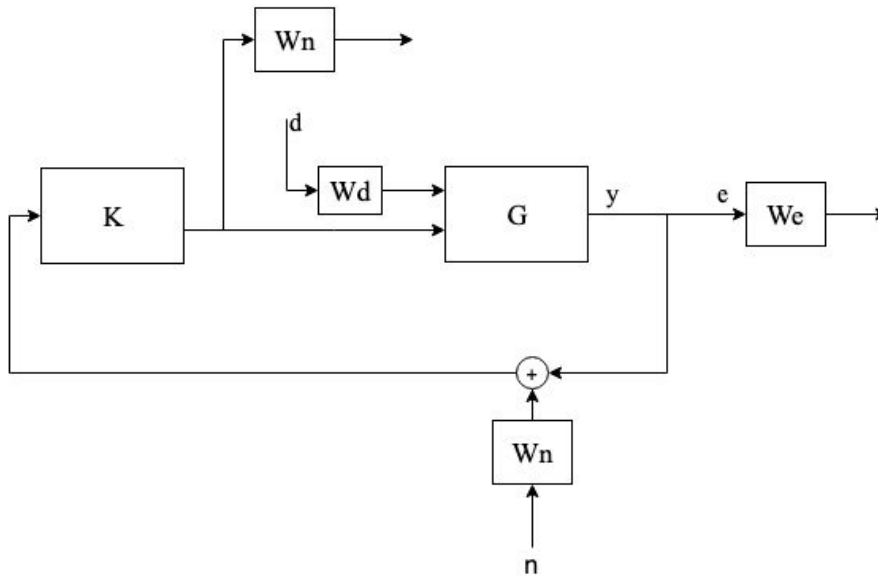

Figure 2.5: $\mathcal{H}_\infty$ control system including weights.

To include frequency dependent weighting factors, first order filters are designed. The transfer function is given by [18], [19] :

$$H(s) = \frac{a_1 s + a_0}{s + \omega_0} \tag{2.46}$$

With a pole at $s = -\omega_0$, a zero at $s = -\frac{a_0}{a_1}$ and a high frequency gain that approaches a_1. It should be noted that the numerator coefficients $(a_0, a1)$ specify the filter type , in a way that if $\frac{a_0}{a_1} > 1$ it becomes a high pass filter, while if $0 < \frac{a_0}{a_1} < 1$ then it becomes a low pass filter [18].

3

System Model and Actuators

This chapter describes the assumed analytical linear representation for the car mechanical system. First, the quarter car model is introduced. The quarter car concept is useful to understand the full car model that is presented later. In the end, how the actuators are modelled as forces in the system is explained. The modeling of the actuators and the applications of the forces is explained.

3.1   Passive Quarter Car Model

The quarter car model is a 2 DOF mechanical system that describes the relation between car body, wheel and road in a car suspension. This model features two bodies: unsprung mass and sprung mass. The unsprung mass represents one wheel part of the suspension and the foundation brakes, moves together with the wheel. The unsprung mass has 1 DOF, which is the vertical translation. Moreover, the unsprung mass interacts with the road through a linear spring-damper parallel system, which describes the forces generated at the tire. The sprung mass represents a share of a quarter car body plus the share of suspension structure that, moves together with the car body. The sprung mass has 1 DOF, which is the vertical translation [20], [21]. Sprung and unsprung mass interact through the car suspension system, which is modelled with a spring and a damper. Figure 3.1 shows the quarter car model. Variables and constants for a passive quarter car model are illustrated in Table 3.1.

Table 3.1: Description of the parameters in the passive quarter car model for a passive suspension system

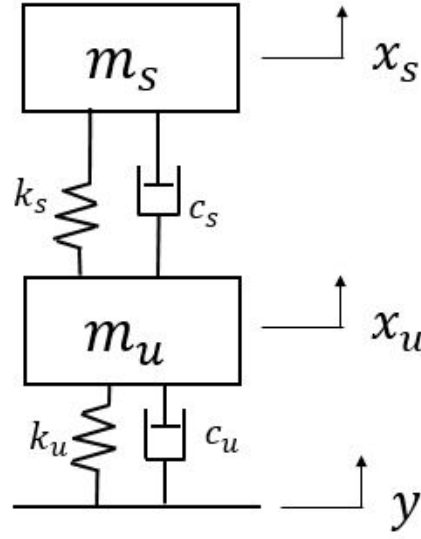| Symbol	Quantity	Unit
m_s	Sprung mass	kg
m_u	Unsprung mass	kg
k_s	Spring stiffness, suspension	N/m
k_u	Spring stiffness, tire	N/m
c_s	Damping coefficient, suspension	Ns/m
c_u	Damping coefficient, tire	Ns/m
x_s	Vertical displacement of sprung mass, heave	m
x_u	Vertical displacement of unsprung mass	m
y	Road height	m

Figure 3.1: Passive quarter car

The equation of the dynamics for a passive quarter car model are formulated as [20]:

$$m_s\ddot{x}_s = -k_s(x_s - x_u) - c_s(\dot{x}_s - \dot{x}_u) \tag{3.1}$$

$$m_u\ddot{x}_u = k_s(x_s - x_u) + c_s(\dot{x}_s - \dot{x}_u) - k_u(x_u - y) - c_u(\dot{x}_u - \dot{y}) \tag{3.2}$$

which can be expressed in matrix form:

$$[M]\ddot{x} + [C]\dot{x} + [K]x = F \tag{3.3}$$

$$\begin{bmatrix} m_s & 0 \\ 0 & m_u \end{bmatrix} \begin{bmatrix} \ddot{x}_s \\ \ddot{x}_u \end{bmatrix} + \begin{bmatrix} c_s & -c_s \\ -c_s & c_s + c_u \end{bmatrix} \begin{bmatrix} \dot{x}_s \\ \dot{x}_u \end{bmatrix} + \begin{bmatrix} k_s & -k_s \\ -k_s & k_s + k_u \end{bmatrix} \begin{bmatrix} x_s \\ x_u \end{bmatrix} = \begin{bmatrix} 0 \\ k_u y + c_u \dot{y} \end{bmatrix} \tag{3.4}$$

3.2 Full Car Model

This section describes a full car model with active suspension actuators, that are modelled through a force element applied between each unsprung mass and the sprung mass. In other words, passive dampers are replaced with active dampers and the anti-roll bars are not modelled in this project. The chassis is considered parallel to the road and the geometry of the suspension system is ignored. Variables and constants for the full car model are illustrated in Table 3.2.

Table 3.2: Parameter description in full car model with active suspension

Symbol	Quantity	Unit
z	Body vertical displacement	m
θ	Body roll angle	rad
ϕ	Body pitch angle	rad
z_{fl}	Front left wheel vertical displacement	m
z_{fr}	Front right wheel vertical displacement	m
z_{rl}	Rear left wheel vertical displacement	m
z_{rr}	Rear right wheel vertical displacement	m
z_{rfl}	road height at front left wheel	m
z_{rfr}	Road height at front right wheel	m
z_{rrl}	Road height at rear left wheel	m
z_{rrr}	Road height at rear right wheel	m
M	Sprung mass	kg
m_{fl}, m_{fr}	Front unsprung masses	kg
m_{rl}, m_{rr}	Rear unsprung masses	kg
k_f	Front suspension spring stiffness	N/m
k_r	Rear suspension spring stiffness	N/m
k_{tf}, k_{tr}	Front and rear tires stiffness	N/m
I_x	Longitudinal mass moment of inertia	kgm^2
I_y	Lateral mass moment of inertia	kgm^2
l_f	Front coil spring longitudinal distance	m
l_r	Rear coil spring longitudinal distance	m
t_l	Left coil spring lateral distance	m
t_r	Right coil spring lateral distance	m
$F_{act,fl}$	Front left sprung mass force	N
$F_{act,fr}$	Front right sprung mass force	N
$F_{act,rl}$	Rear left sprung mass force	N
$F_{act,rr}$	Rear right sprung mass force	N
F_{tfl}	Front left unsprung mass force	N
F_{tfr}	Front right unsprung mass force	N
F_{trl}	Rear left unsprung mass force	N
F_{trr}	Rear right unsprung mass force	N

The 7 DOF model, used to represent the complete vehicle, is illustrated in figure 3.2. Its 7 degrees of freedom consist of heave, roll and pitch of the car body, plus the vertical motion of the unsprung mass for each quarter. The vertical displacements and velocities of each quarter of the chassis are described as [20]:

$$z_{fl}(t) = z(t) - l_f sin(\phi(t)) + t_l sin(\theta(t)) \tag{3.5}$$

$$z_{fr}(t) = z(t) - l_f sin(\phi(t)) - t_r sin(\theta(t)) \tag{3.6}$$

$$z_{rl}(t) = z(t) + l_r sin(\phi(t)) + t_l sin(\theta(t)) \tag{3.7}$$

$$z_{rr}(t) = z(t) + l_r sin(\phi(t)) - t_r sin(\theta(t)) \tag{3.8}$$

$$\dot{z}_{fl}(t) = \dot{z}(t) - l_f\dot{\phi}(t)cos(\phi(t)) + t_l\dot{\theta}(t)cos(\theta(t)) \tag{3.9}$$

$$\dot{z}_{fr}(t) = \dot{z}(t) - l_f\dot{\phi}(t)cos(\phi(t)) - t_r\dot{\theta}(t)cos(\theta(t)) \tag{3.10}$$

$$\dot{z}_{rl}(t) = \dot{z}(t) + l_r\dot{\phi}(t)cos(\phi(t)) + t_l\dot{\theta}(t)cos(\theta(t)) \tag{3.11}$$

$$\dot{z}_{rr}(t) = \dot{z}(t) + l_r\dot{\phi}(t)cos(\phi(t)) - t_r\dot{\theta}(t)cos(\theta(t)) \tag{3.12}$$

Figure 3.2: 7 DOF full car model

The model is linearized by using small angle approximation, where $sin(\phi) \approx \phi$ and $cos(\phi) \approx 1$:

$$z_{fl}(t) = z(t) - l_f\phi(t) + t_l\theta(t) \tag{3.13}$$

$$z_{fr}(t) = z(t) - l_f\phi(t) - t_r\theta(t) \tag{3.14}$$

$$z_{rl}(t) = z(t) + l_r\phi(t) + t_l\theta(t) \tag{3.15}$$

$$z_{rr}(t) = z(t) + l_r\phi(t) - t_r\theta(t) \tag{3.16}$$

$$\dot{z}_{fl}(t) = \dot{z}(t) - l_f\dot{\phi}(t) + t_l\dot{\theta}(t) \tag{3.17}$$

$$\dot{z}_{fr}(t) = \dot{z}(t) - l_f\dot{\phi}(t) - t_r\dot{\theta}(t) \tag{3.18}$$

$$\dot{z}_{rl}(t) = \dot{z}(t) + l_r\dot{\phi}(t) + t_l\dot{\theta}(t) \tag{3.19}$$

$$\dot{z}_{rr}(t) = \dot{z}(t) + l_r\dot{\phi}(t) - t_r\dot{\theta}(t) \tag{3.20}$$

From the Newton's law, equations of equilibrium are derived as follows:

$$M\ddot{z}(t) = -F_{fl}(t) - F_{fr}(t) - F_{rl}(t) - F_{rr}(t) \tag{3.21}$$

19

$$I_x\ddot{\theta}(t) = (F_{rr}(t) + F_{fr}(t))t_r - (F_{rl}(t) + F_{fl}(t))t_l + M_R \tag{3.22}$$

$$I_y\ddot{\phi} = (F_{fl}(t) + F_{fr}(t))l_f - (F_{rl}(t) + F_{rr}(t))l_r \tag{3.23}$$

$$m_{fl}\ddot{z}_{fl}(t) = F_{fl}(t) - F_{tfl}(t) \tag{3.24}$$

$$m_{fr}\ddot{z}_{fr}(t) = F_{fr}(t) - F_{tfr}(t) \tag{3.25}$$

$$m_{rl}\ddot{z}_{rl}(t) = F_{rl}(t) - F_{trl}(t) \tag{3.26}$$

$$m_{rr}\ddot{z}_{rr}(t) = F_{rr}(t) - F_{trr}(t) \tag{3.27}$$

The sprung mass forces are defined as:

$$F_{fl}(t) = k_f(z_{fl}(t) - z_{tfl}(t)) - F_{act,fl}(t) \tag{3.28}$$

$$F_{fr}(t) = k_f(z_{fr}(t) - z_{tfr}(t)) - F_{act,fr}(t) \tag{3.29}$$

$$F_{rl}(t) = k_r(z_{rl}(t) - z_{trl}(t)) - F_{act,rl}(t) \tag{3.30}$$

$$F_{rr}(t) = k_r(z_{rr}(t) - z_{trr}(t)) - F_{act,rr}(t) \tag{3.31}$$

Unsprung masses forces are defined as follows:

$$F_{tfl}(t) = k_{tf}(z_{tfl}(t) - z_{rfl}(t)) \tag{3.32}$$

$$F_{tfr}(t) = k_{tf}(z_{tfr}(t) - z_{rfr}(t)) \tag{3.33}$$

$$F_{trl}(t) = k_{tr}(z_{trl}(t) - z_{rrl}(t)) \tag{3.34}$$

$$F_{trr}(t) = k_{tr}(z_{trr}(t) - z_{rrr}(t)) \tag{3.35}$$

3.3 Actuator Model

Four individual active dampers are used in the models. The actuators are active so their models are assumed to be linear in order to design linear controllers based on LTI systems. Hence, the resulting forces from the active dampers are equal to the controlled forces from the specific controller as follows:

$$\begin{aligned} F_{ctrl,fl}(t) &= F_{act,fl}(t) \\ F_{ctrl,fr}(t) &= F_{act,fr}(t) \\ F_{ctrl,rl}(t) &= F_{act,rl}(t) \\ F_{ctrl,rr}(t) &= F_{act,rr}(t) \end{aligned} \tag{3.36}$$

Active damper model is illustrated in figure 3.3.
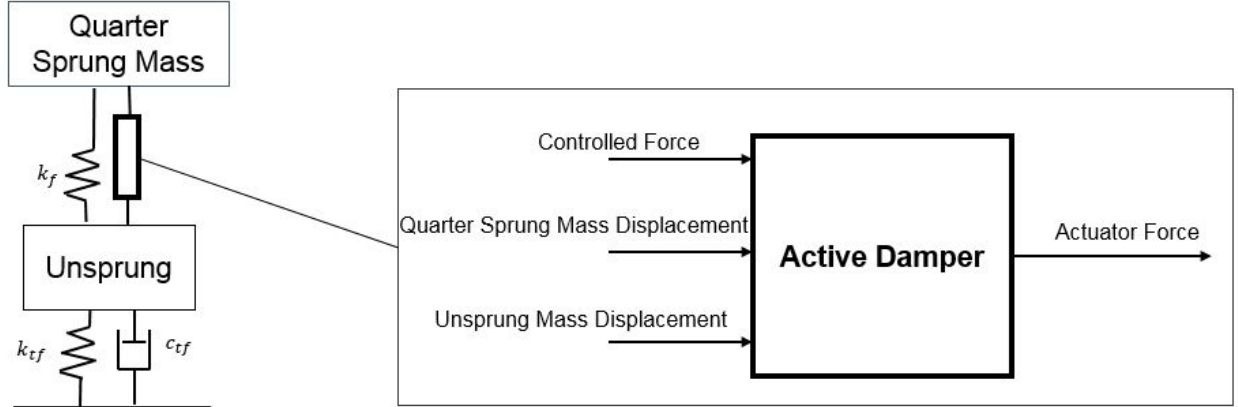
Figure 3.3: Active damper model

3.4 State space representation

The linearized full car model derived in section 3.2, provided with four active dampers, is described by a state space representation. The state space is written as:

$$\dot{x}(t) = Ax(t) + Bu(t) + B_\omega \omega(t) \tag{3.37}$$

$$y(t) = Cx(t) + Du(t) + D_\omega \omega(t) \tag{3.38}$$

Where $\mathbf{x}(t)$ is the state vector, $\mathbf{u}(t)$ is the control signal vector and $\omega(t)$ is the disturbance input signal vector. These vectors are defined as follows:

$$\mathbf{x}(t) = \left[z, \dot{z}, \phi, \dot{\phi}, \theta, \dot{\theta}, z_{fl}, \dot{z}_{fl}, z_{fr}, \dot{z}_{fr}, z_{rl}, \dot{z}_{rl}, z_{rr}, \dot{z}_{rr}\right]^T \tag{3.39}$$

$$\mathbf{u}(t) = \left[u_1, u_2, u_3, u_4\right]^T = \left[F_{act,fl}, F_{act,fr}, F_{act,rl}, F_{act,rr}\right] \tag{3.40}$$

$$\omega(t) = \left[w_1, w_2, w_3, w_4\right]^T \tag{3.41}$$

The initial values ($t_0 = 0$) of state variables are defined as zeros:

$$\mathbf{x}(t_0) = \left[0, 0, 0, 0, 0, 0, 0, 0, 0, 0, 0, 0, 0, 0\right]^T \tag{3.42}$$

3.5 Ride Comfort

Ride comfort is associated to the overall comfort and well-being of passengers when traveling in a vehicle. The main sources of discomfort are the car body oscillations, sensed as noises and vibrations. The sources of these oscillations are outside the vehicles compartment. Active and passive components are used to prevent these irregularities to be transmitted to the occupants in the vehicle [2]. For ride evaluation, there have been studies to find the excitation frequency intervals which human body is more sensitive to. However, ride comfort plays a key role when the high-end customer is purchasing a car [22]. In this regard, car manufacturers are improving the comfort using high technology suspension components.

3.6 Suspension System

The suspension system characteristics affect ride comfort and handling. In order to improve ride comfort, reduction of roll, pitch and vertical accelerations is desired. Ride comfort can be improved by using active or semi-active suspension control. In this thesis, passive springs and active dampers are used. Semi-active damper will be described first for getting better overview of active damper.

3.6.1 Passive Suspension

In a passive suspension system, there is no additional force. Other than the forces generated by passive dampers and passive springs. The springs convert road profile disturbances to potential energy. The dampers dissipate energy to damp out disturbances.

In a passive suspension, there is an approximately linear relation between force and deflection velocity of the damper where $F_{damp} = -cv_{def}$. c is the damping coefficient. Actually, the linear approximation is valid for low deflection velocities only. Figure 3.4 and 3.5 shows passive damper with linear approximation characteristics and more accurate nonlinear characteristics respectively [8].
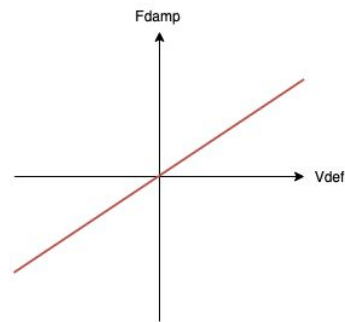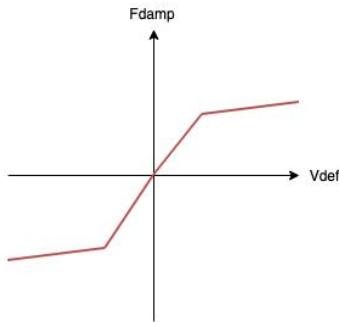
Figure 3.4: Nonlinear passive damper   **Figure 3.5:** Linear passive damper

3.6.2 Semi-active Suspension

In order to get a trade-off between ride comfort and handling, passive dampers need to be tuned. In this regards, semi-active dampers and active dampers are used since they have the possibility to control the force exerted by the actuators [8]. Semi-active dampers coefficients vary between within certain amount of bandwidth (shown in figure 3.6 and 3.7). They can only dissipate energy, not add energy. So the control forces cannot be chosen independently, with respect to the damper velocity.
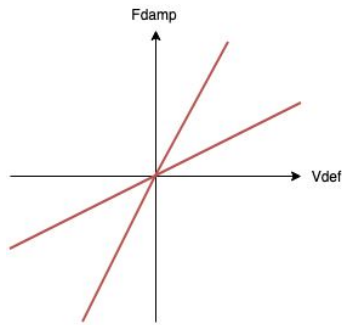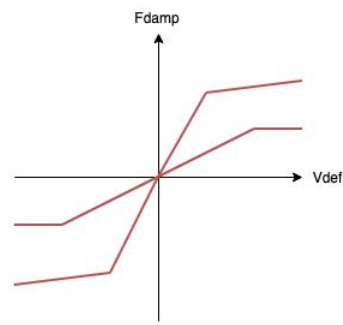
Figure 3.6: Linear semi active

Figure 3.7: Nonlinear semi active

3.6.3 Active Suspension

Active suspension can both add energy to the system or dissipate energy from it. Forces applied by active actuators are independent of damper velocity [8]. Therefore, the force generated by an active suspension system are not dependant on the relative velocity between the vehicle and wheels. Active damper characteristics is shown in figure 3.8.
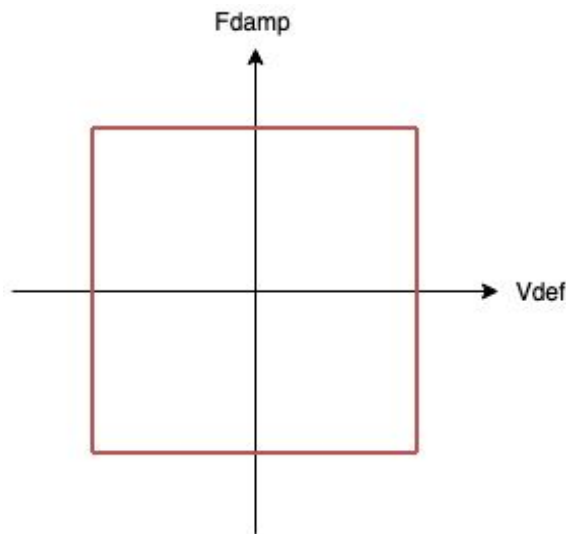

Figure 3.8: Active damper

3.6.4 Anti-Roll Bars

Anti-roll bars provide roll moment to counteract the vehicle roll angle, for example during cornering maneuvers [7].
Passive anti-roll bars connect opposite wheels of the car body and act as torsion springs.
Active anti-roll bars react differently based on different road conditions. In active anti-roll bars, the bar is split between the two wheels and the two branches are connected by an actuator that generates the torque.

4

Implementation

4.1 Control Implementation and Weighting Factor Selection

All three controllers are linear. Active dampers are able to produce forces at anytime. The designed controllers are meant to provide the system with desired controlled forces.

In the following sections, weighting factor selection procedures for sky-hook, LQR and $\mathcal{H}_\infty$ controllers are presented.

4.1.1 Sky-hook Controller Implementation

To implement the sky-hook controller, the four actuators forces, the four quarter car velocities and the four wheels velocities are considered in the controller design. Deflection velocity in a quarter is defined as the difference between body local vertical velocity and wheel vertical velocity in a specific quarter. Body velocities on each quarters have been introduced in (3.17), (3.18), (3.19) and (3.20). The wheel velocities, which are the derivatives of the wheel displacements.

Based on its limitations, each active damper can generate forces that are bounded between minimum and maximum forces called F_{min} and F_{max}, respectively.

$$F_{act,fl}(t) = \begin{cases} F_{max,fl} & \dot{z}_{fl}(t)(\dot{z}_{fl}(t) - \dot{z}_{tfl}(t)) > 0 \\ F_{min,fl} & \dot{z}_{fl}(t)(\dot{z}_{fl}(t) - \dot{z}_{tfl}(t)) = 0 \end{cases} \tag{4.1}$$

$$F_{act,fr}(t) = \begin{cases} F_{max,fr} & \dot{z}_{fr}(t)(\dot{z}_{fr}(t) - \dot{z}_{tfr}(t)) > 0 \\ F_{min,fr} & \dot{z}_{fr}(t)(\dot{z}_{fr}(t) - \dot{z}_{tfr}(t)) = 0 \end{cases} \tag{4.2}$$

$$F_{act,rl}(t) = \begin{cases} F_{max,rl} & \dot{z}_{rl}(t)(\dot{z}_{rl}(t) - \dot{z}_{trl}(t)) > 0 \\ F_{min,rl} & \dot{z}_{rl}(t)(\dot{z}_{rl}(t) - \dot{z}_{trl}(t)) = 0 \end{cases} \tag{4.3}$$

$$F_{act,rr}(t) = \begin{cases} F_{max,rr} & \dot{z}_{rr}(t)(\dot{z}_{rr}(t) - \dot{z}_{trr}(t)) > 0 \\ F_{min,rr} & \dot{z}_{rr}(t)(\dot{z}_{rr}(t) - \dot{z}_{trr}(t)) = 0 \end{cases} \tag{4.4}$$

In order to apply reasonable forces based on different situation, forces must vary. So the forces change as the body quarters velocities and wheels velocities change.

In this project, minimum forces on car quarters are not large in magnitude due to the fact that car is suspended on springs. All four quarters have the same constant minimum forces value as follows,

$$
\begin{aligned}
F_{min,fl} &= F_{min} \\
F_{min,fr} &= F_{min} \\
F_{min,rl} &= F_{min} \\
F_{min,rr} &= F_{min}
\end{aligned}
\tag{4.5}
$$

On the other hand, the maximum forces can vary, due to the conditions mentioned in the equations above. So the maximum forces are functions of time. To design a suitable function for the maximum force, the constants c_1 and c_2 have been used to make a trade-off between deflection velocities and wheel velocities as follows,

$$
\begin{aligned}
F_{max,fl}(t) &= c_1(\dot{z}_{fl}(t) - \dot{z}_{tfl}(t)) + c_2\dot{z}_{fl}(t) \\
F_{max,fr}(t) &= c_1(\dot{z}_{fr}(t) - \dot{z}_{tfr}(t)) + c_2\dot{z}_{fr}(t) \\
F_{max,rl}(t) &= c_1(\dot{z}_{rl}(t) - \dot{z}_{trl}(t)) + c_2\dot{z}_{rl}(t) \\
F_{max,rr}(t) &= c_1(\dot{z}_{rr}(t) - \dot{z}_{trr}(t)) + c_2\dot{z}_{rr}(t)
\end{aligned}
\tag{4.6}
$$

4.1.2 Sky-hook Weighting Factor Selection

About the selection of the correct weightings c_1 and c_2, the active dampers limitation regarding the maximum forces should be taken into account to generate the desired forces in different road scenarios. The constants c_1 and c_2 can be selected based on the values of the damping coefficients in the passive damper and the tire damping coefficient respectively.

4.1.3 LQR Implementation

It is straightforward to design linear LQR controller for active dampers. Figure 4.1 shows the closed loop control structure for LQR controller.
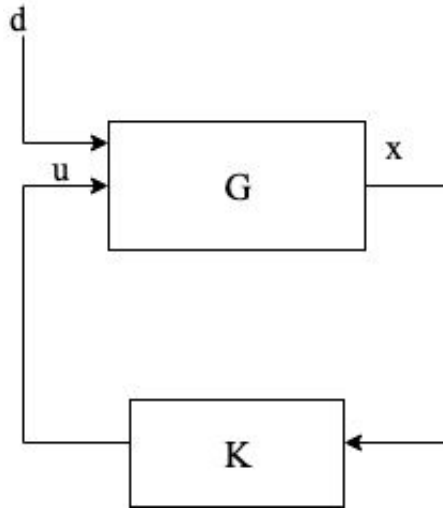
Figure 4.1: LQR controller illustration. Block 'G' is the system plant.'x' is the state vector. 'u' is the active dampers forces vector. 'd' is the road profile.

In the implementation of the LQR controller, a high pass filter has been applied to some of the states in order to feed the controller with proper signals and, in the end, to calculate the desired control gain K_{LQR}. The penalized states are heave displacement and all four wheels displacements. The main reason to use the high pass filter is to set up the controller so that it will not generate constant forces in a scenario with constant road height.

4.1.4 LQR Weighting Factor Selection

Regarding the weight factor selection for Q and R matrices in LQR controller, based on ride comfort target, the penalties are set on heave acceleration, roll acceleration and pitch acceleration. Also roll rate has to be penalized more than pitch rate. Hence, it is necessary to prioritize states for the control objective, which is ride comfort.

4.1.5 $\mathcal{H}_\infty$ Implementation

The $\mathcal{H}_\infty$ controller is synthesized based on the generalized plant G and the active damper. The control structure is illustrated in figure 4.2.

In the $\mathcal{H}_\infty$ controller algorithm the suspension deflection of each quarter, heave acceleration, roll acceleration and pitch acceleration are output by the plant G, so that all these seven system states can be penalized in error. Hence, the number of measured states are 21 states.

The suspension deflection is the difference between the local body displacement and wheel displacement in each quarter, as defined below in (4.7).

$$z_{def,fl}(t) = z_{fl}(t) - z_{tfl}(t)$$
$$z_{def,fr}(t) = z_{fr}(t) - z_{tfr}(t)$$
$$z_{def,rl}(t) = z_{rl}(t) - z_{trl}(t)$$
$$z_{def,rr}(t) = z_{rr}(t) - z_{trr}(t)$$

(4.7)
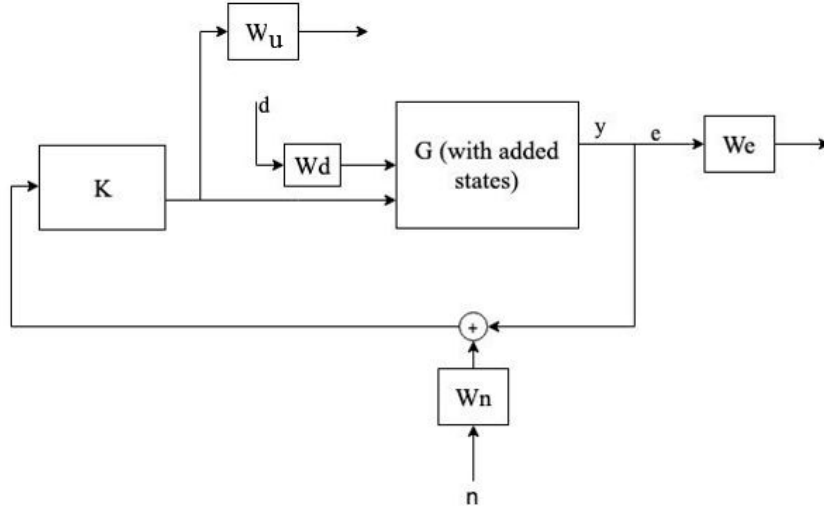
Figure 4.2: $\mathcal{H}_\infty$ control system including weights.

4.1.6 $\mathcal{H}_\infty$ Weighting Factor Selection

The active dampers are bandwidth limited and the objective is to improve the ride comfort. Considering these, first order filters are designed. High-pass filters and low-pass filters try to keep the control gain at low level for high frequencies. Following low-pass filter is the weighting function for the deflection rate of the four car quarters:

$$LP = \frac{s + \omega_0}{0.001s + \omega_0}$$

(4.8)

A first order high-pass filter is used to penalize heave acceleration, roll acceleration and pitch acceleration:

$$HP = \frac{s + 2\omega_0}{s + 0.01\omega_0}$$

(4.9)

Where ω_0 is the frequency of measured states. To penalize roll rate and pitch rate, a low pass filter (with specified low-frequency gain, crossover frequency and high-frequency gain) is used.
To calculate the control effort weighting function, a low pass filter, similar to the one defined in the (4.8), is used. The noise weight block is the noise measurement on the system outputs. This block maps the unmeasured noise on each measured states.

The maximum noise values considered for angles and angles rates are:

$$W_{n,roll} = 0.01\frac{\pi}{180}, W_{n,pitch} = 0.01\frac{\pi}{180} \tag{4.10}$$

Where $W_{n,roll}$ is the weight for roll, roll rate and roll acceleration and $W_{n,pitch}$ is the weight for pitch, pitch rate and pitch acceleration.
The maximum noise values considered for wheels displacements, car heave, wheels velocities, car heave rate and car heave acceleration are:

$$W_{n,z} = 0.01, W_{n,wheel} = 0.01 \tag{4.11}$$

Where $W_{n,z}$ is the weight for car heave, car heave rate and car heave acceleration and $W_{n,wheel}$ is the weight for wheel displacements and wheel velocities.
The maximum noise value for suspension deflections is:

$$W_{n,def} = 0.5 \tag{4.12}$$

In (4.13), the road disturbance weight is set as the upper bound of road input variation:

$$W_d = 0.05 \tag{4.13}$$

4.2 Model Verification

This section is describing model verification of the system. It presents model verification of the 7 DOF analytical model through comparison with IPG CarMaker realistic model. This comparison is done through a road profile with heave, roll and pitch excitation to verify the alignments of the states behaviour in both models. This is to compare the full car model in MATLAB to the realistic vehicle model in CarMaker. So the system states are read from CarMaker and there is the state space block to read the states variables from MATLAB. The car has passive suspension with constant damping coefficients.
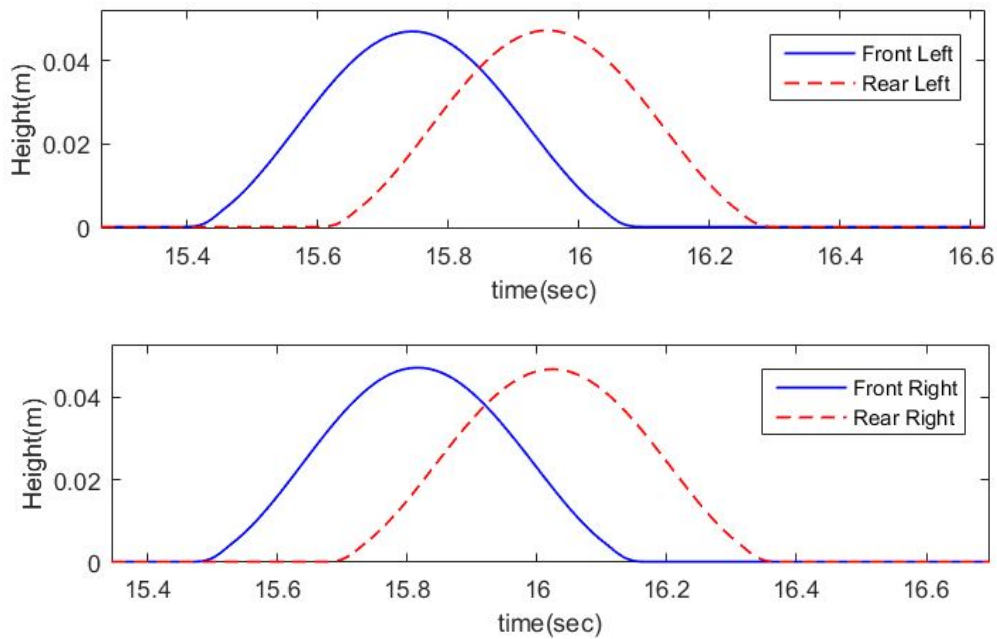
Figure 4.3: Road profile for verifying analytical representation of the full car. The blue curves show the front wheels road profiles on left side and right side respectively. The red curves show the rear wheels road profiles on left side and right side respectively.

A test case has been designed: the road profile features a single wave with a height of $5cm$. The wave is slightly offset for left and right side of the car, so that it excites heave, pitch and roll motion: the front left wheel hits the wave first, then the front right wheel hits it, and the sequence will be the same for following rear wheels; hence, there are different bumps on the left and right side. It should be noted that in this simulation the car longitudinal speed is constant and set to $50km/h$. The full car model has been described in section 3.2. Figure 5.1. shows the road profile used in the verification simulation.
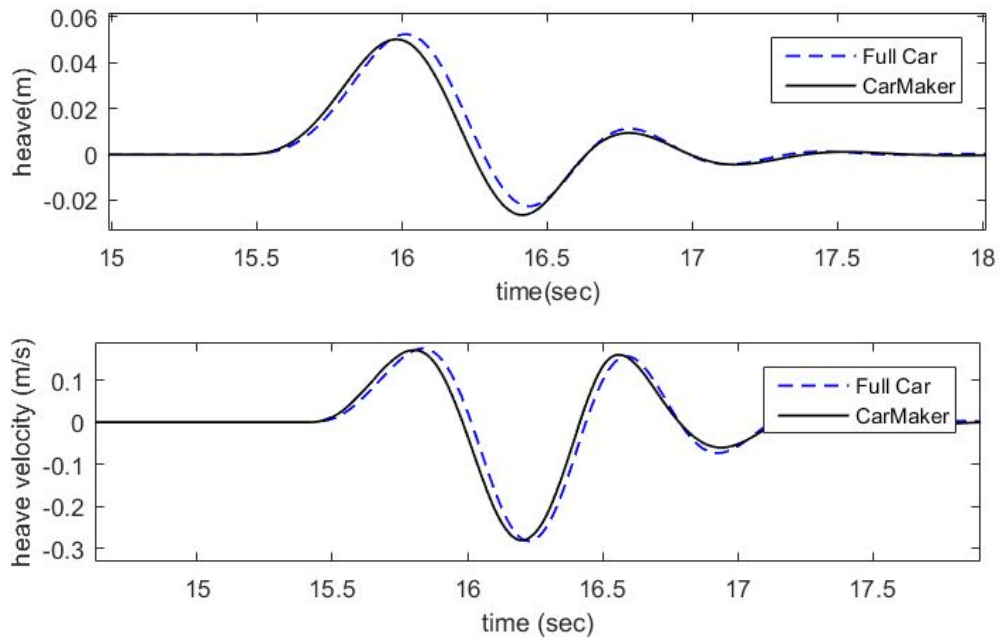
Figure 4.4: Heave and heave velocity comparisons between full car model and CarMaker model
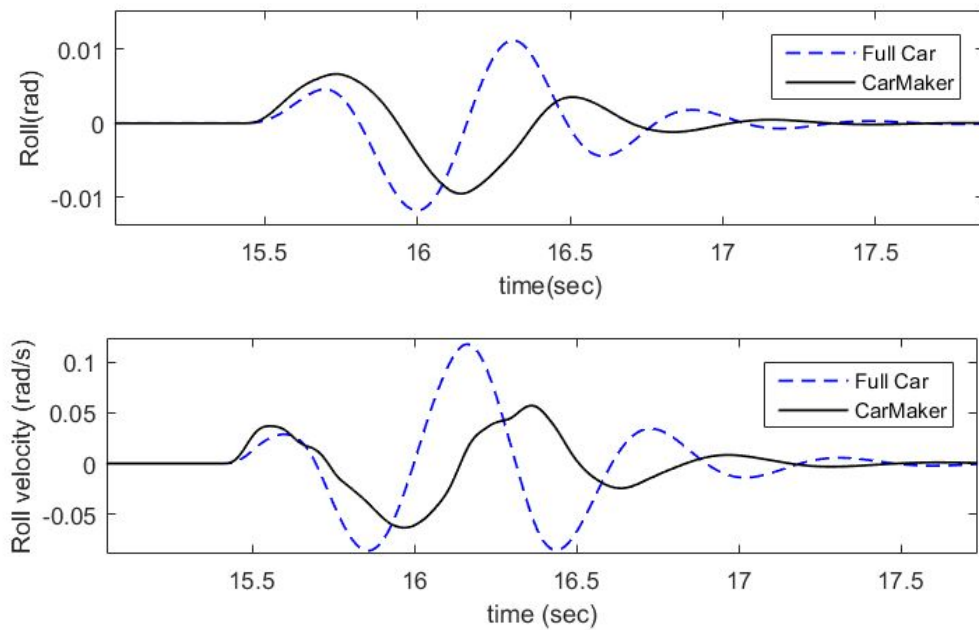
Figure 4.5: Roll and roll velocity comparisons between full car model and Car-Maker model
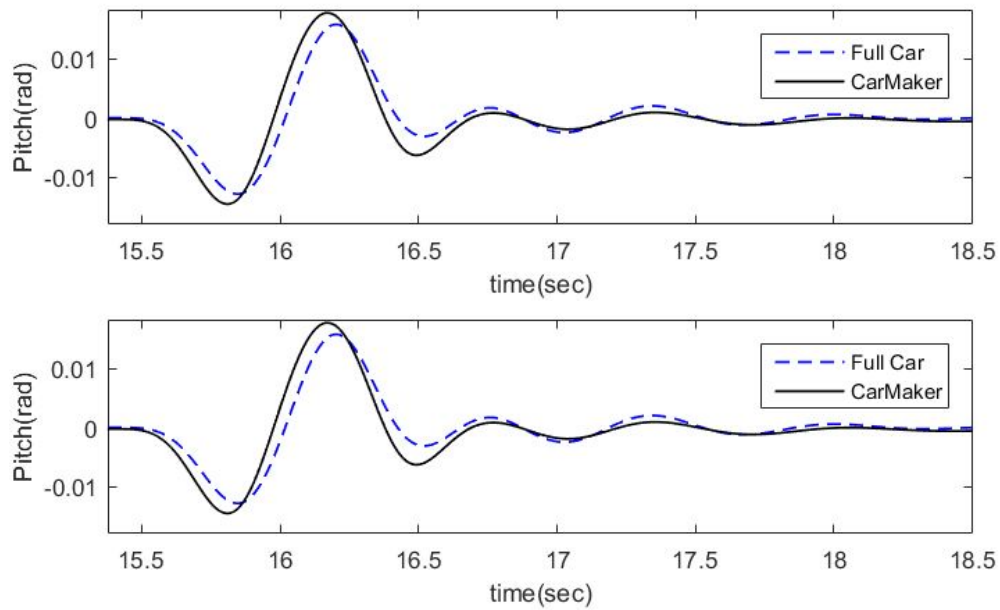
Figure 4.6: Pitch and pitch velocity comparisons between full car model and CarMaker model
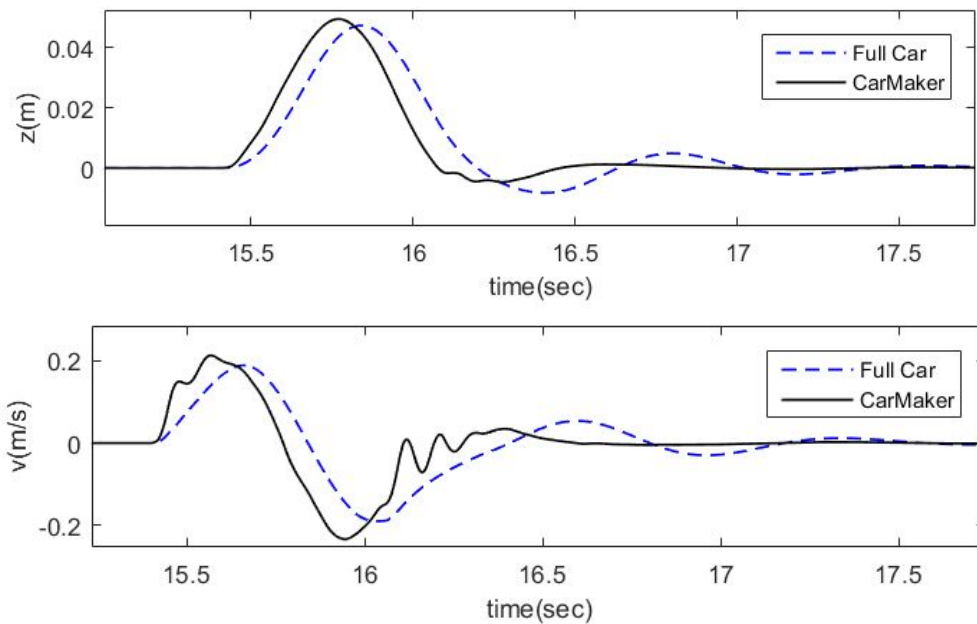
Figure 4.7: Front left wheel displacement and its velocity comparisons between full car model and CarMaker model

Based on results in figures 4.4, 4.5, 4.6 and 4.7, it can be seen that both models showed similar behaviour. There are some slight differences between full car model and realistic model from CarMaker. The analytical full car model in MATLAB has 7 DOF only including heave, roll, pitch and 4 DOF of wheel vertical translations, while the model in IPG CarMaker features a full kinematics and compliance characterization that results in a more accurate representation of the suspension behaviour

4. Implementation

and there can be seen differences can be seen in comparisons. Also, the anti-roll bars are not modelled in full car model. In general, curves shapes look like each other and the major differences are in amplitudes.

In analytical full car model from MATLAB, the tire forces are modelled with spring-damper parallel systems which are connected to the road profile directly.

5

Results

This project aims to improve ride comfort. Hence, the objective is to design a suitable control method for controlling active dampers. The optimization goal is to find control forces for the actuators in order to minimize the car body accelerations, including vertical acceleration $\ddot{z}$, roll acceleration $\ddot{\phi}$ and pitch acceleration $\ddot{\theta}$. The reference values for evaluation of roll, roll rate, roll acceleration, pitch, pitch rate and pitch acceleration are set as zero. Heave acceleration, roll acceleration and pitch acceleration are evaluated to investigate the ride comfort.

5.1 Control Performance

Four different standard test cases are introduced to test control methods, sky-hook, LQR and $\mathcal{H}_\infty$. The road scenarios include heave, pitch and roll excitations which are sufficient to test the controller performances. The comparisons are presented on the same figure together with the passive suspension system. Controllers are implemented through IPG CarMaker for a realistic simulation environment. IPG CarMaker is a virtual test environment for passenger cars.
Controllers performances are analyzed through the following test cases:

1. Ramp
2. One side disturbance
3. Unsymmetrical waves
4. FEC track

The actuator are represented by realistic active damper models with electrohydraulic characteristics. In an electrohydraulic actuator, the damping coefficients can be changed by modifying the size of the orifices.
To evaluate performances between different controllers together with the passive suspension system, the Root Mean Square of the body accelerations is used.

$$a_{RMS} = \sqrt{\frac{1}{n}(a_1^2 + a_2^2 \cdots + a_n^2)} \qquad (5.1)$$

For a more clear of showing the results of the matrices improvements in different
controller where the RMS error are calculated as:

$$control_{improvement} = \frac{passive_{RMS} - control_{RMS}}{passive_{RMS}} * 100\% \qquad (5.2)$$

The power spectral density of body accelerations using Fast Fourier Transform
method is also calculated to analyze the frequency content.

5.1.1 Ramp

Ramp is a simple test case with high frequency characteristics. This test case is a
good start to evaluate general performances of the systems such as transient response
and disturbance reduction. The excitation is a sudden upside ramp with positive
slope followed by a sudden downside ramp with negative slope after a proper distance
as shown in figure 5.1. The vehicle has a proper amount of time to reduce the ramp
disturbance. The parameters describing the scenario can be seen in Table 5.1.

Table 5.1: Parameters for the ramp test case

Parameter	value
Speed,v_x	50 Km/h
Ramp length	42 m
Ramp height	0.04 m
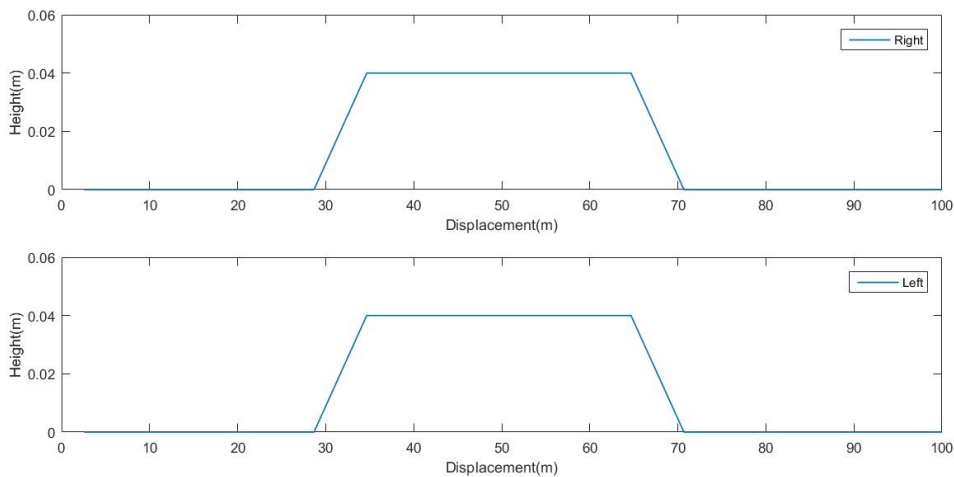
Figure 5.1: Ramp road profile

The RMS errors for different controllers compared to the passive are summarized
in Table 5.2. Since the road excitation is on heave motion and pitch motion, the

related figures and RMS errors are presented.RMS errors show positive values in state acceleration which have made improvements in terms of the ride comfort.

Table 5.2: RMS errors during ramp test case

Parameter	Sky-hook	LQR	$\mathcal{H}_\infty$
Heave	0.02%	0.001%	0.01%
Heave vel	27.8 %	42.2 %	35.32%
Heave acc	36.36%	64.45%	43.91 %
Pitch	4.86 %	18.4%	12.71%
Pitch vel	28.61%	47.95%	-5.2%
Pitch acc	15.95%	40.15%	-17.81%
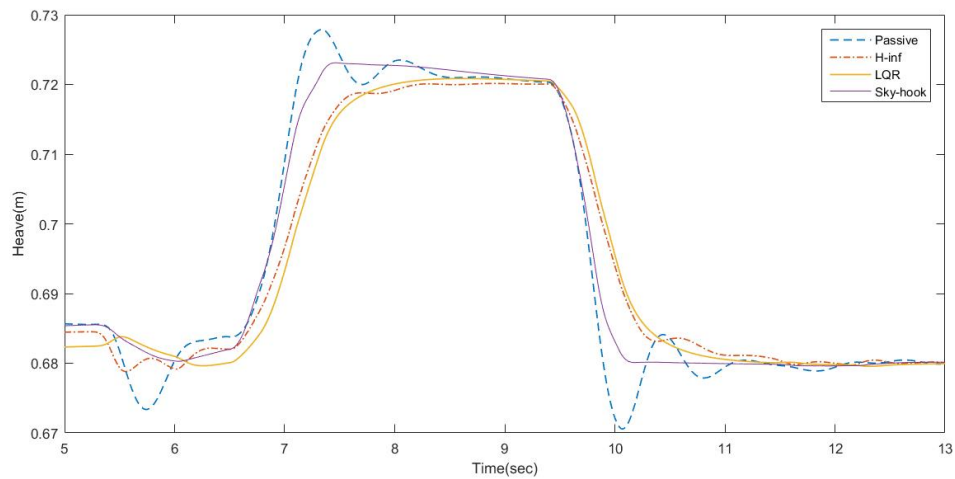
Figure 5.2: Heave response for the ramp test case
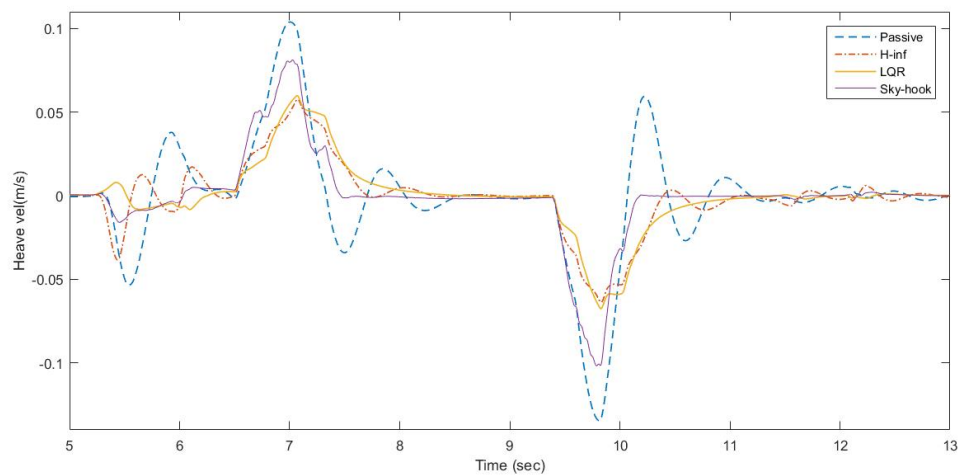
Figure 5.3: Heave velocity response for the ramp test case

As it can be seen in figure 5.2, heave amplitude is decreased for all active suspension systems compared to the passive suspension system. All 3 controllers do not experience any overshoots and there is no transient response.

It can be seen that the LQR controller reacts better than other controllers during this test case. There is a smooth response when it comes to the road disturbances. Figure 5.3 shows the heave velocity of different systems. All the controllers have improved the Heave velocity significantly. They have reduced the oscillations and show smooth controller responses. In this case, the $\mathcal{H}_\infty$ and the LQR controller results are better. Sky-hook controller shows high frequency oscillations with smaller amplitudes that can negatively affect the ride comfort.
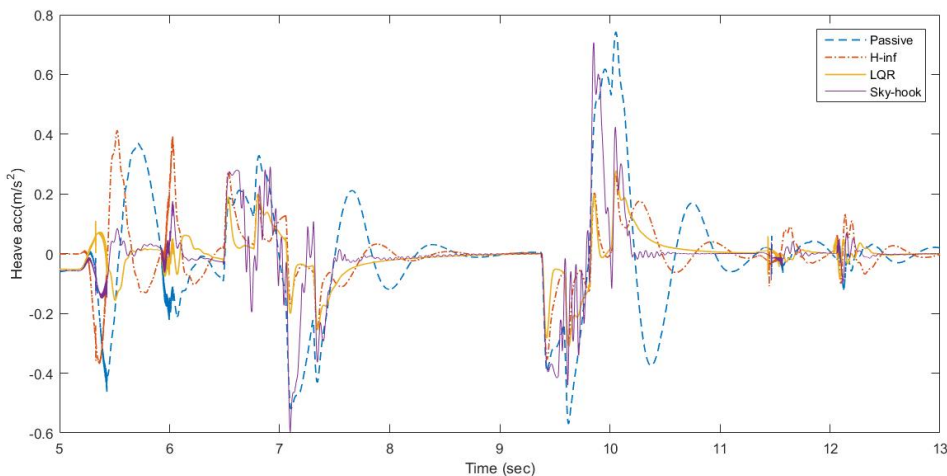
Figure 5.4: Heave acceleration response for the ramp test case

The heave acceleration in figure 5.4, is decreased for amplitude in all the controllers. They show a good reduction of acceleration disturbances as well as the fast transient response. Although sky-hook controller shows positive improvement in RMS error, it oscillates a lot with high frequency which is not an acceptable response for the ride comfort target. It can be seen that the $\mathcal{H}_\infty$ controller performs well in terms of tracking but it reacts slower than it is expected. However LQR controller shows the best result among these controllers with fast response, good disturbance attenuation.
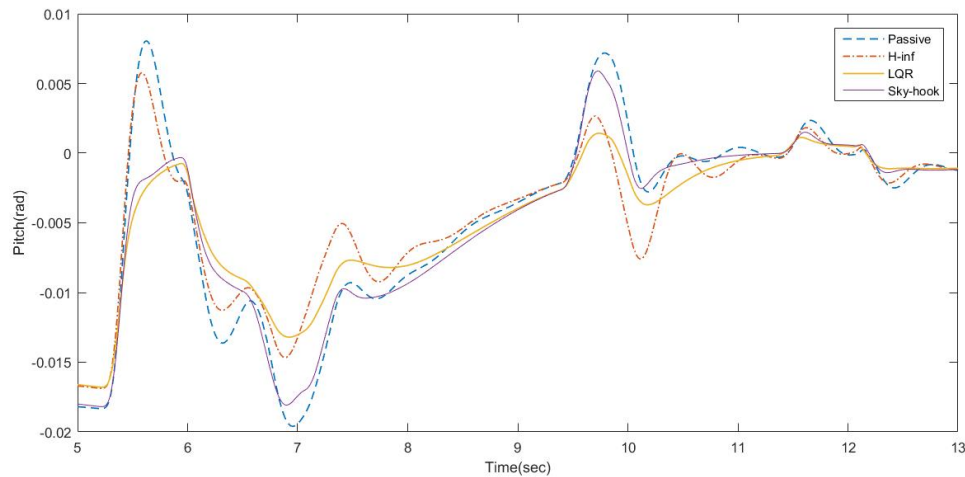
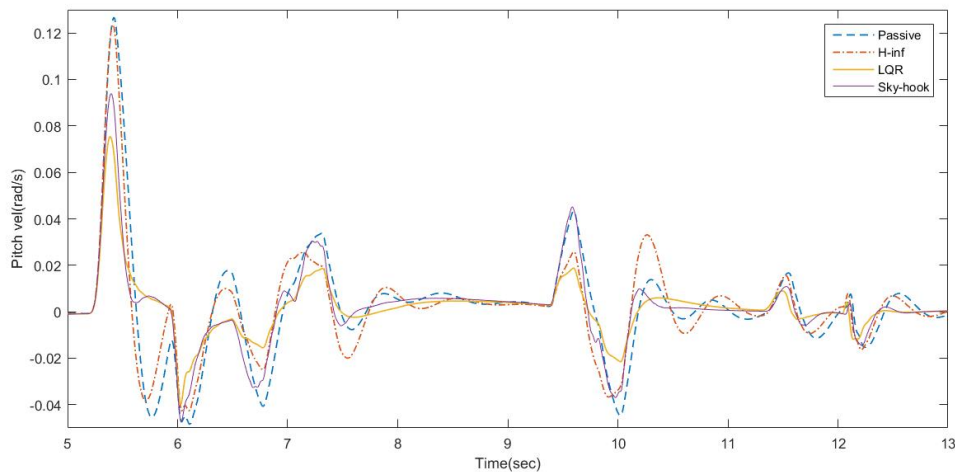**Figure 5.5:** Pitch angle for the ramp test case

Figure 5.6: Pitch velocity for the ramp test case

As it can be seen in figure 5.5 the pitch angle has been improved for all the controllers comparing to the passive. In this case, the response speed showed the same level. LQR and shy-hook decay faster than passive and LQR mitigates pitch disturbance better than the other controllers.

The LQR controller quickly reduces the disturbance in the pitch angle and shows smooth response. Also, the transient response is the shortest.

In terms of pitch velocity in figure 5.6, with slight decreases for the active systems compared to the passive one, the controlled systems damp out the oscillations faster. Major improvement in damping out the oscillations for the sky-hook and the LQR can be seen. The $\mathcal{H}_\infty$ controller shows the same damping result as the passive one.
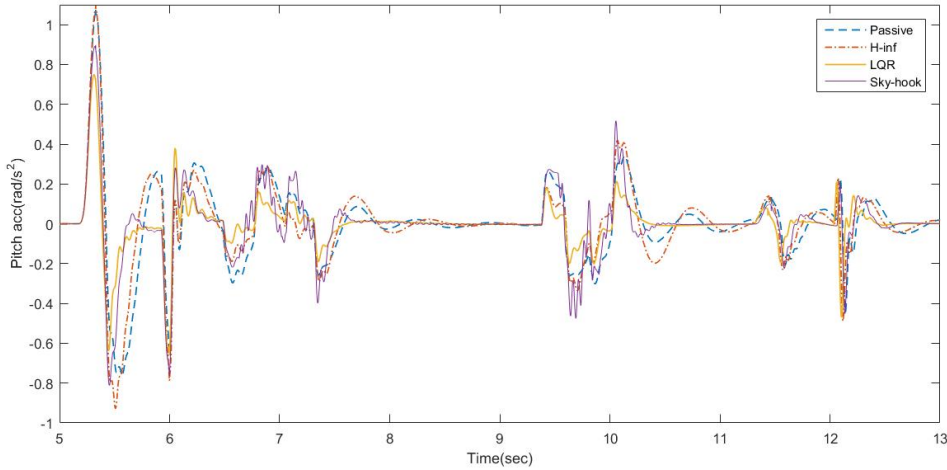
Figure 5.7: Pitch acceleration for the ramp test case

Pitch acceleration is shown in figure 5.7. In pitch acceleration, controlled systems react faster to road disturbances and they oscillate less than the passive system to mitigate road excitations. LQR controller shows a promising result. Although $\mathcal{H}_\infty$ controller has experienced negative RMS errors, it has better tracking compared to sky-hook controller. Sky-hook controller shows high frequency oscillations for disturbance rejection that are not acceptable for ride comfort.

5.1.2 One Side Disturbance

In this scenario, a one sided disturbance is investigated. The car is exposed to an excitation on the left side in shape of a wave, while the road on the right side is a flat profile as shown in figure 5.8. This test case is an interesting scenario since the resulting disturbances affect roll, pitch and heave at the same time. Parameters defining the test case are presented in Table 5.3.

The calculated RMS errors of the controlled systems compared to the passive system, are summarized in Table 5.4. There can be seen major RMS error improvements in car body accelerations for all the controllers.

Table 5.3: Parameters for the one side disturbance test case

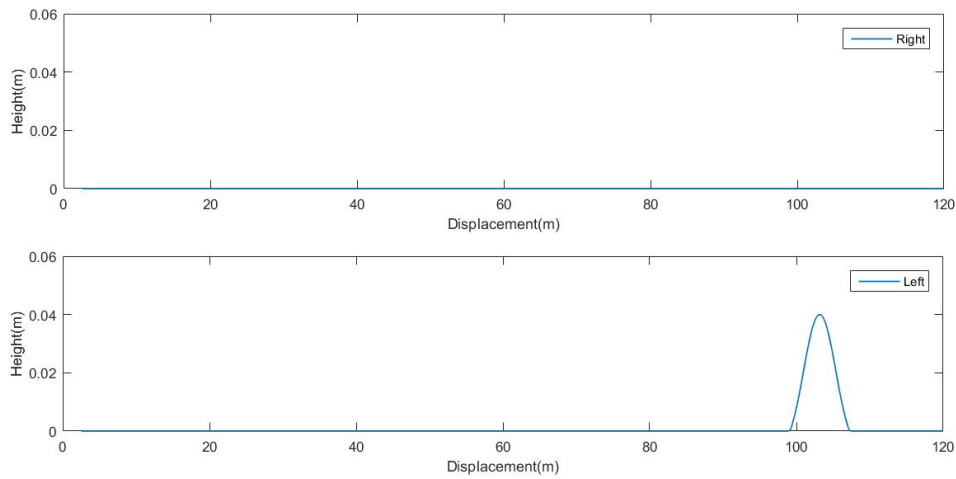| Parameter	value
Speed,v_x	50 Km/h
Left side bump length	9 m
Left side bump height	0.04 m

Figure 5.8: One side disturbance road profile

Table 5.4: RMS errors during one side disturbance test case

Parameter	Sky-hook	LQR	$\mathcal{H}_\infty$
Heave	0.076%	0.087%	0.073%
Heave vel	63.29%	77.8 %	71.4%
Heave acc	59%	80.68%	71.46 %
Pitch	22.73 %	25.54%	-23.01%
Pitch vel	26.71%	41.71%	-22.05%
Pitch acc	-16.34%	2.36%	-50.89%
Roll	40.21 %	31.05%	22.44%
Roll vel	0%	-38%	-72.4%
Roll acc	50.36%	38.6%	21.7%
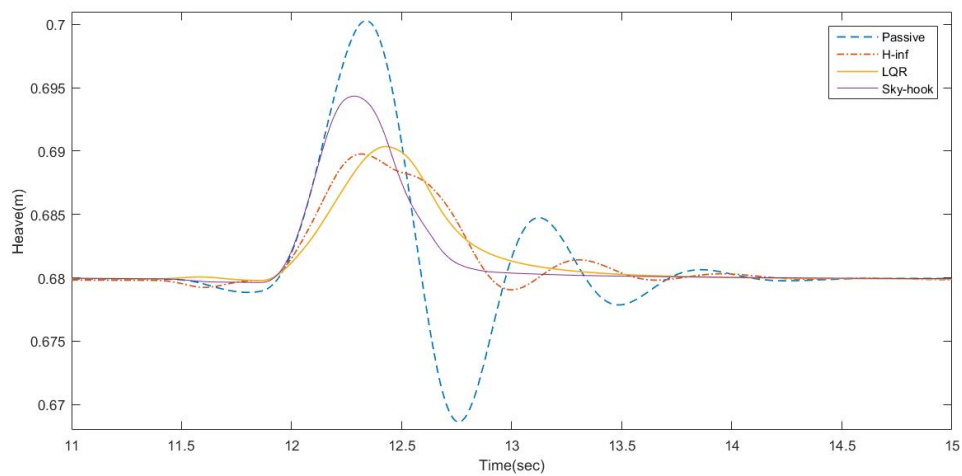
Figure 5.9: Heave response for the one side disturbance test case
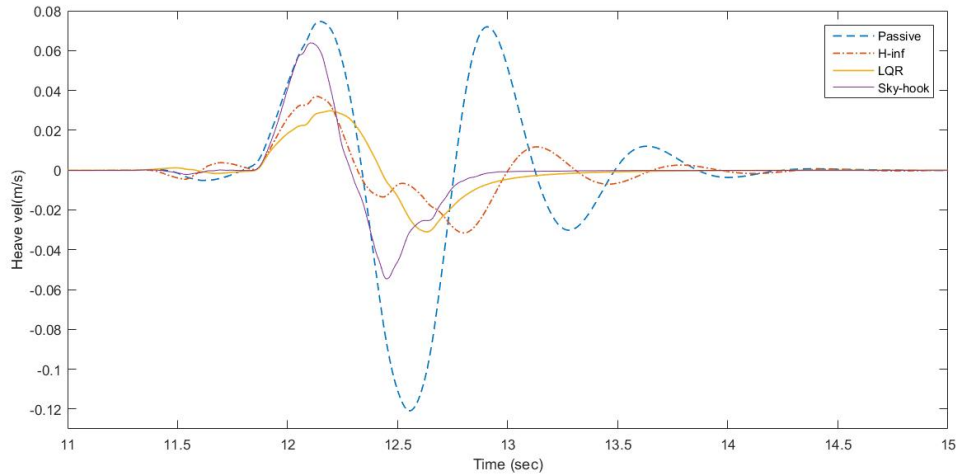
Figure 5.10: Heave velocity response for the one side disturbance test case

Based on RMS errors of heave responses, the controlled systems have experienced the same RMS values as the passive system. However, in the figure 5.9, for controlled systems show smaller amplitudes and smoother transient responses comparing to the passive suspension. Hence, ride comfort target is improved in this test case. LQR and $\mathcal{H}_\infty$ have minimized the heave accelerations better than sky-hook.

It can be seen in figure 5.10 that the heave velocities show a significant improvement on amplitudes as well as the oscillations reduction. The LQR controller has a fast response to the disturbance and keeps the signal close to zero more effectively.
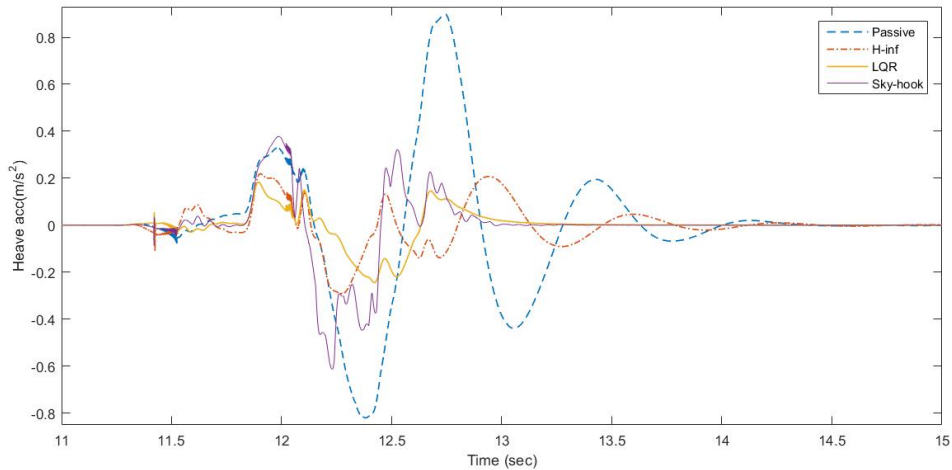
Figure 5.11: Heave acceleration response for the one side disturbance test case

There can be seen in figure 5.11 a significant decrease in heave acceleration peak values for all the controlled systems and they over all damp out the disturbances faster than the passive system. LQR has the best disturbance attenuation compared to all the systems. $\mathcal{H}_\infty$ shows smoother results compared to the sky-hook control system.
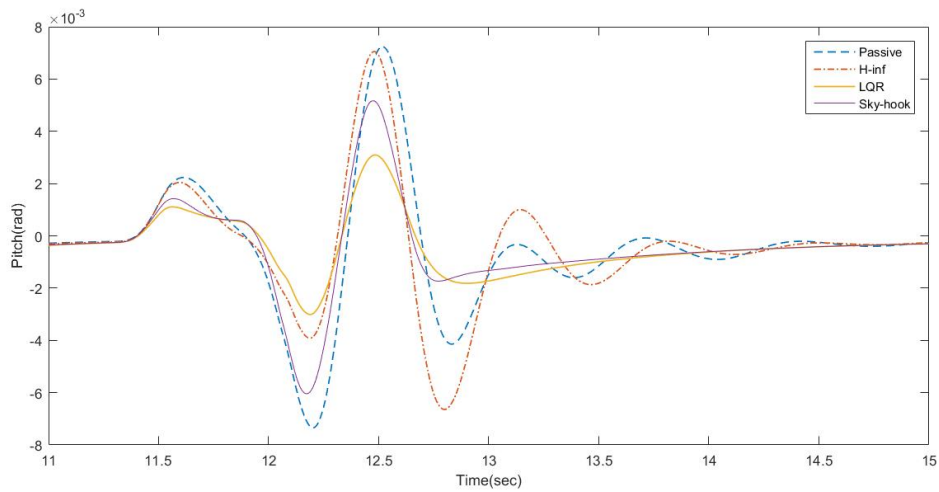
40

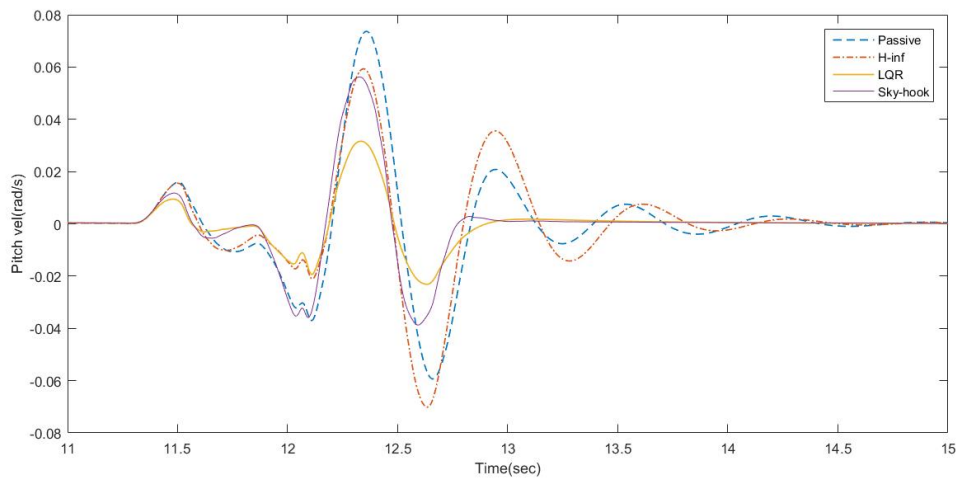**Figure 5.12:** Pitch angle for the one side disturbance test case

Figure 5.13: Pitch velocity for the one side disturbance test case

In case of pitch angle and pitch velocity in figure 5.12 and figure 5.13, the LQR and the sky-hook controllers result in decreased amplitudes and they damped out the oscillations faster than the passive system. However, $\mathcal{H}_\infty$ is not able to damp the oscillations as expected and it follows the same shape as the passive system.
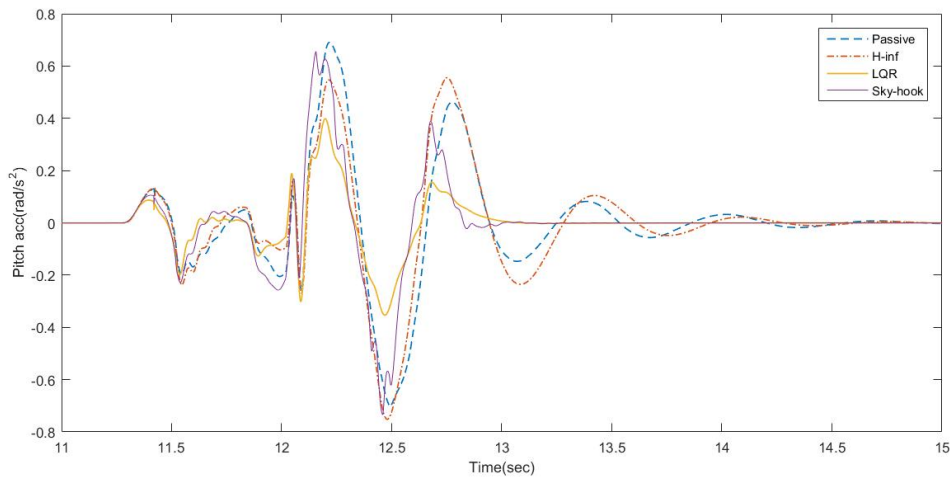
Figure 5.14: Pitch acceleration for the one side disturbance test case

The pitch acceleration is showed in figure 5.14. Based on the pitch acceleration curves,all controllers show good tracking response with positive RMS errors. However LQR controller shows a very good result in terms of pitch acceleration, which also damps out very well the second overshoot compared to the passive suspension. $\mathcal{H}_\infty$ has smooth response, while sky-hook controller produces more system oscillations.
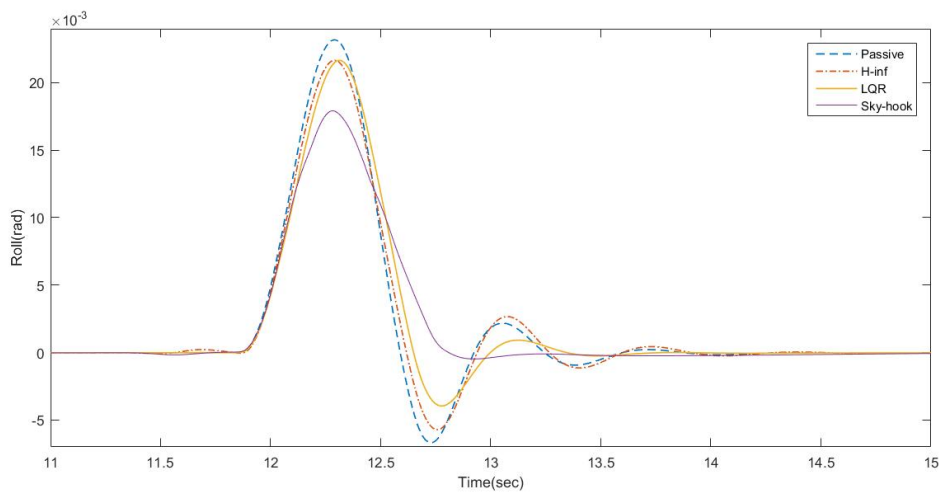
Figure 5.15: Roll angle for the one side disturbance test case
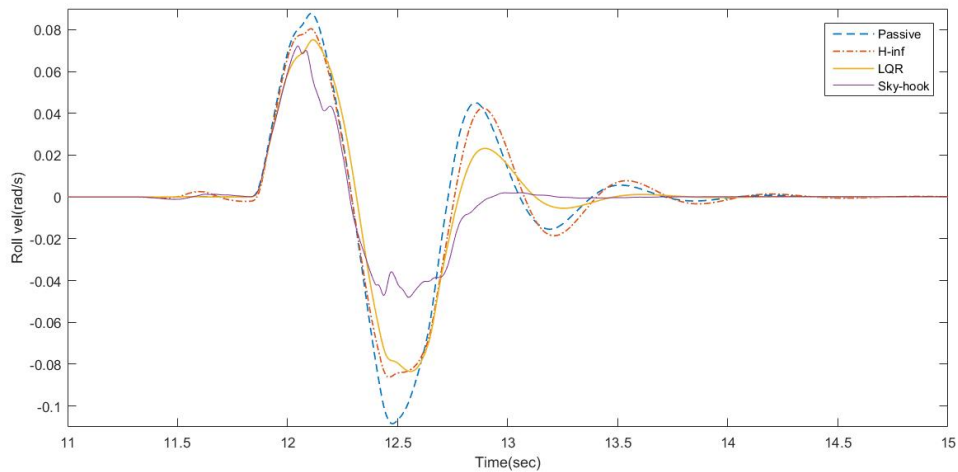
Figure 5.16: Roll velocity for the one side disturbance test case

As shown in figure 5.15 roll angle responses of the controlled systems show approximately same responses for passive suspension, except LQR and sky-hook damp out the overshoots. In figure 5.16 roll velocities have not been improved compared to the passive suspension. Sky-hook shows better attenuation of road disturbance here. Hence, roll accelerations have to be analyzed for conclusion of roll motion response in this case.
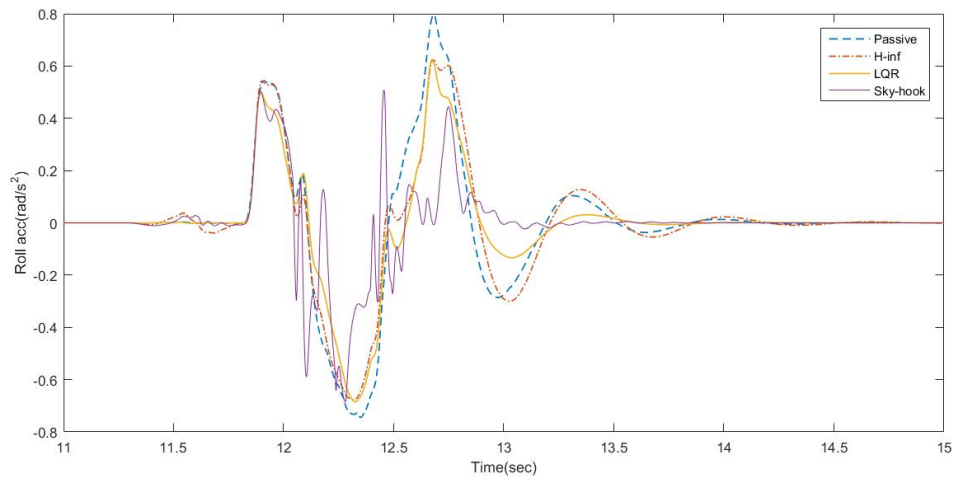

Figure 5.17: Roll acceleration for the one side disturbance test case

In terms of roll acceleration, that can be seen in figure 5.17, major improvements have been achieved. It is also important for the ride comfort target. LQR and $\mathcal{H}_\infty$ control systems decay faster than the passive one and they follow the shape of oscillations of the passive system with decreased roll acceleration magnitudes. The sky-hook controller oscillates more and seems to have difficulties to damp out the roll acceleration: instead it applies extra roll acceleration irregularities to the vehicle body. Hence, in this case, the RMS error is not a good criteria to evaluate the controllers performances, curve shapes have to be considered instead.

5.1.3 Unsymmetrical Waves

As shown in figure 5.18, this test case is defined to excite both the front side and the right side of the vehicle to generate combined roll, pitch and heave excitation. This test case is used to test the roll motion performance in low frequency with different amplitudes. Left and right wheels hit the waves at the same time. But the waves heights have different values on the left and right side, so they are unsymmetrical waves. The test scenario parameters are presented in Table 5.5.

Table 5.5: Parameters for the unsymmetrical waves test case

| Parameter	value
Speed,v_x	50 Km/h
1st left side wave length	9 m
1st left side wave height	0.02 m
1st right side wave length	9 m
1st right side wave height	0.01 m
2nd left side wave length	9 m
2nd left side wave height	0.04 m
2nd right side wave length	9 m
2nd right side wave height	0.03 m
3rd left side wave length	9 m
3rd left side wave height	0.06 m
3rd right side wave length	9 m
3rd right side wave height	0.05 m
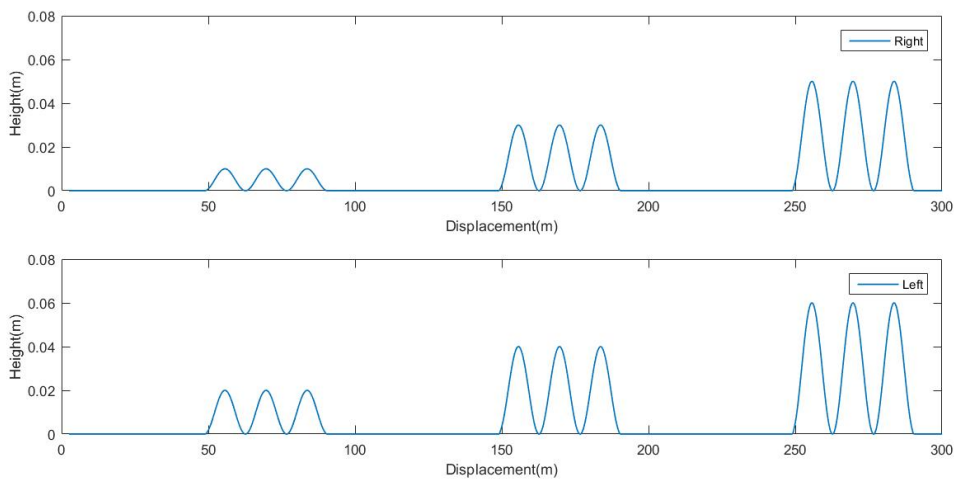
Figure 5.18: Unsymmetrical waves road profile

The RMS errors during unsymmetrical bumps test case are presented in Table 5.6

Table 5.6: RMS errors during unsymmetrical bump test case

Parameter	Sky-hook	LQR	$\mathcal{H}_\infty$
Heave	0.01%	0.002%	0.0034%
Heave vel	44.88%	67.34%	60.82%
Heave acc	46.4%	71%	64.61 %
Pitch	1.89 %	6.64%	-20.20%
Pitch vel	-5.55%	7.97%	-35.34%
Pitch acc	10.50%	13.54%	-20.92%
Roll	16.06%	2.7%	5.28%
Roll vel	0%	-28.2%	-29.25%
Roll acc	-254.03%	12.26%	-3.4%
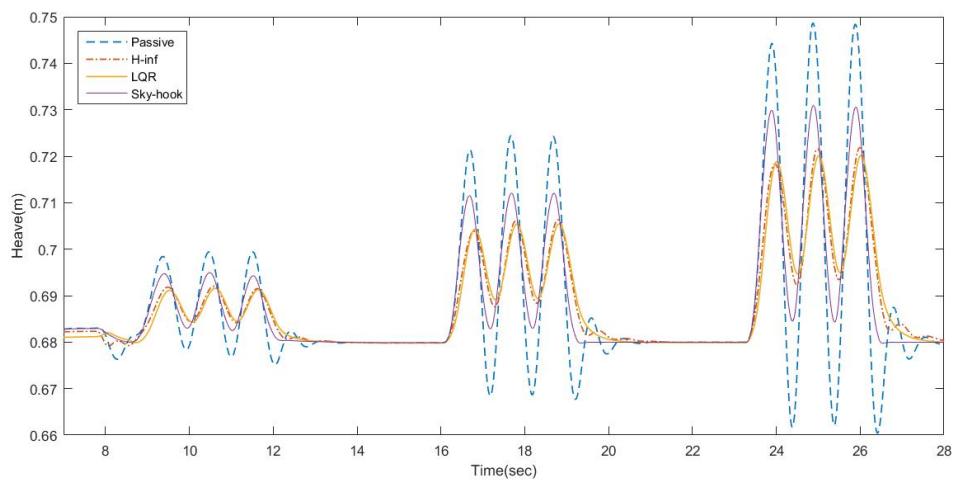
Figure 5.19: Heave response for the unsymmetrical waves test case
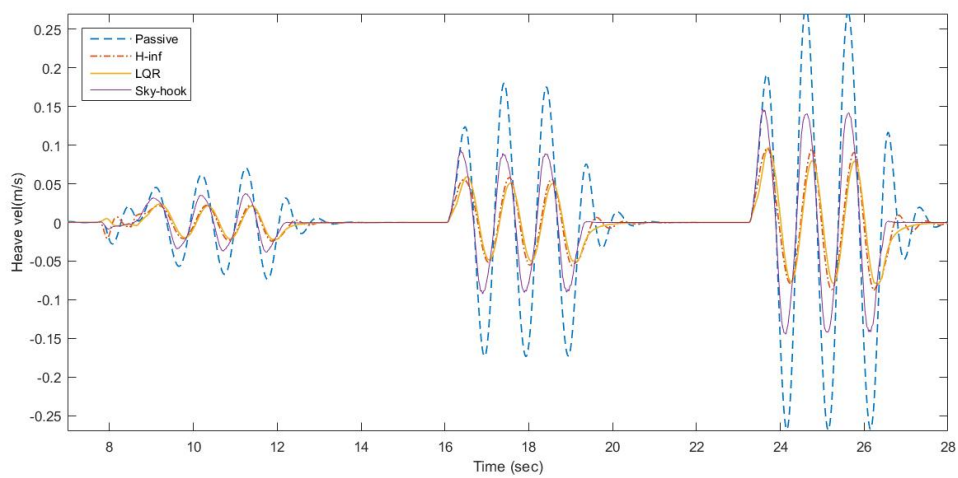
Figure 5.20: Heave velocity for the unsymmetrical waves test case

45

In case of heave displacement and heave velocity that are shown in figure 5.19 and figure 5.20 respectively, the controlled systems experience the same signal shapes as the passive system but decreased amplitudes. RMS error show significant improvements in heave velocity response. Generally, controller have experienced smoother signal tracking.
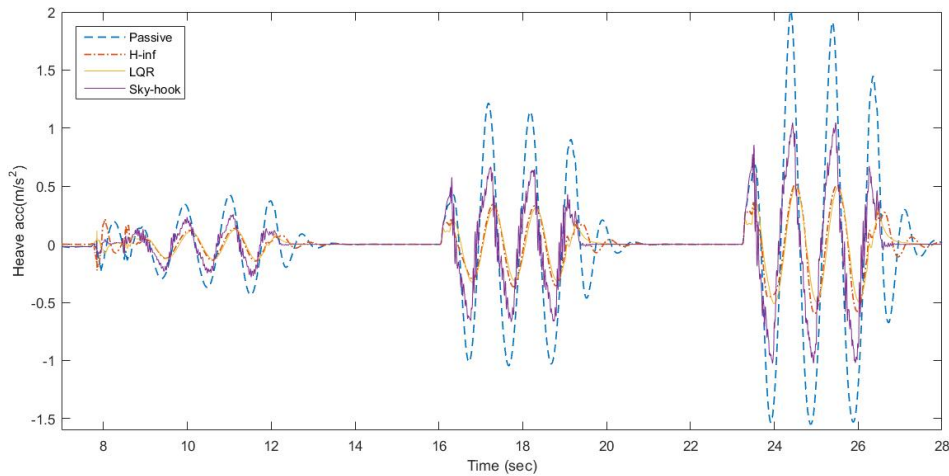

Figure 5.21: Heave acceleration for the unsymmetrical waves test case

Figure 5.21 represents heave acceleration responses. It can be seen that for all the controllers RMS errors show positive responses. Sky-hook has experienced high frequency, low amplitude oscillations when trying to damp out the road disturbances. Instead $\mathcal{H}_\infty$ has smoother results compared to the sky-hook controller. $\mathcal{H}_\infty$ reacts slower than the LQR and sky-hook systems. As shown in heave acceleration response, LQR has the best results in terms of disturbance rejection and response speed.
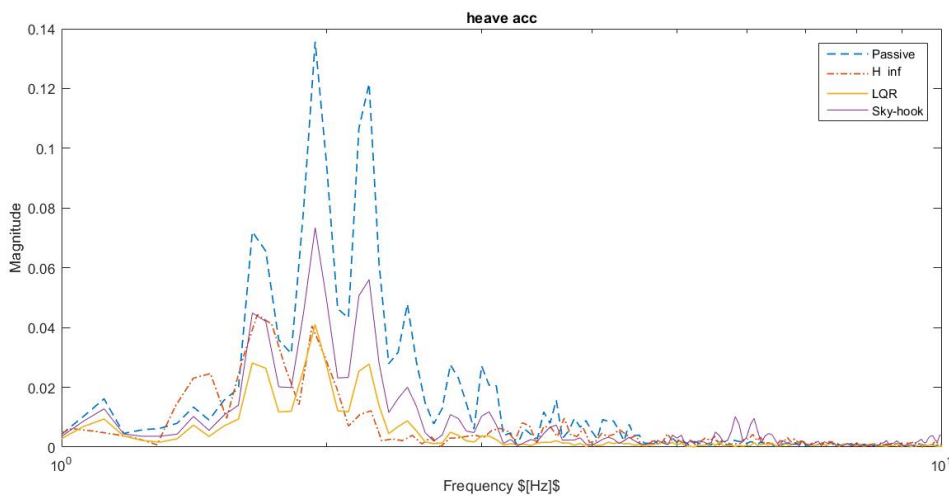

Figure 5.22: Heave acceleration FFT analysis for the unsymmetrical waves test case

Heave acceleration FFT analysis can be seen in figure 5.22. As seen, the magnitude of the frequency content in all the controllers are lower than passive system, which results in better ride comfort performance.
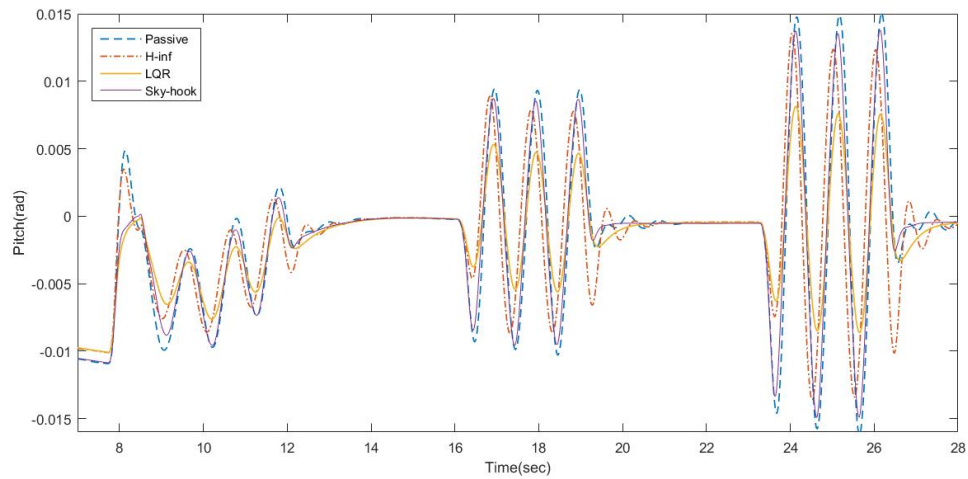

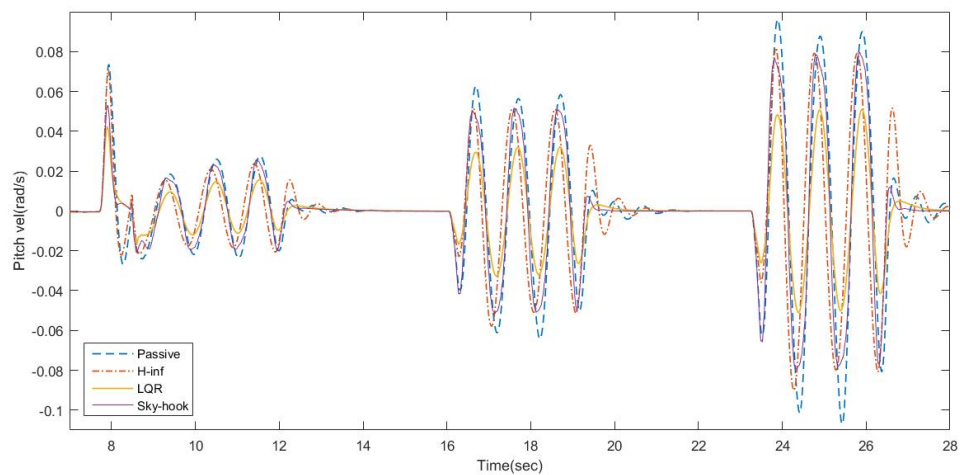**Figure 5.23:** Pitch angle for the unsymmetrical waves test case

Figure 5.24: Pitch velocity for the unsymmetrical waves test case

As seen in figure 5.23 and figure 5.24, pitch and pitch velocity are improved for the LQR and the sky-hook controllers. The $\mathcal{H}_\infty$ controller does not show the expected good results in terms of amplitude decrease and the control system tracks the same behavior as the passive system.

However, regarding the pitch angle, the LQR controller has better performance compared to other controllers, with a smoother response and improved amplitude.
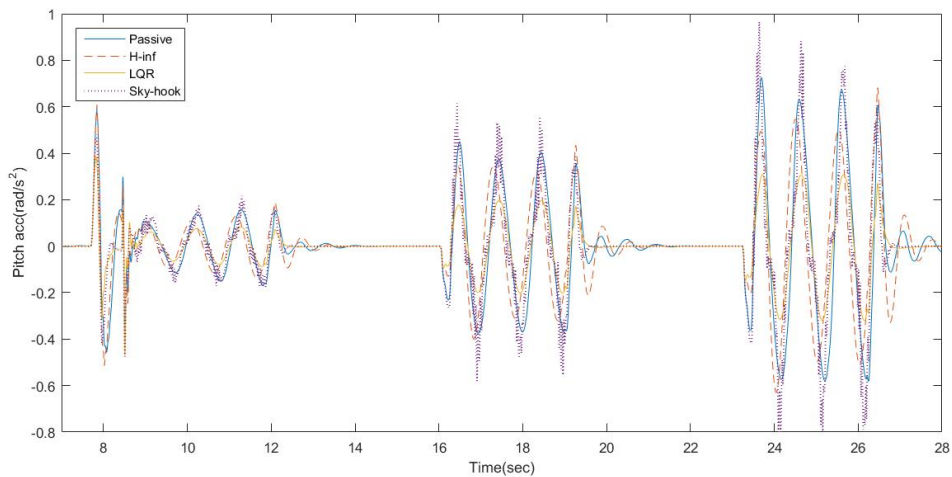
Figure 5.25: Pitch acceleration for the unsymmetrical waves test case

Pitch acceleration seen in figure 5.25 shows decrease of amplitudes for $\mathcal{H}_\infty$ and LQR controllers compared to the passive system. LQR controller mitigates the irregularities better compared to the $\mathcal{H}_\infty$ controller. Instead the sky-hook controller has negative RMS error and shows increase in amplitude compared to the passive system, which is not acceptable for ride comfort. The sky-hook controller amplifies more the roll acceleration amplitudes as the road disturbance height increases.
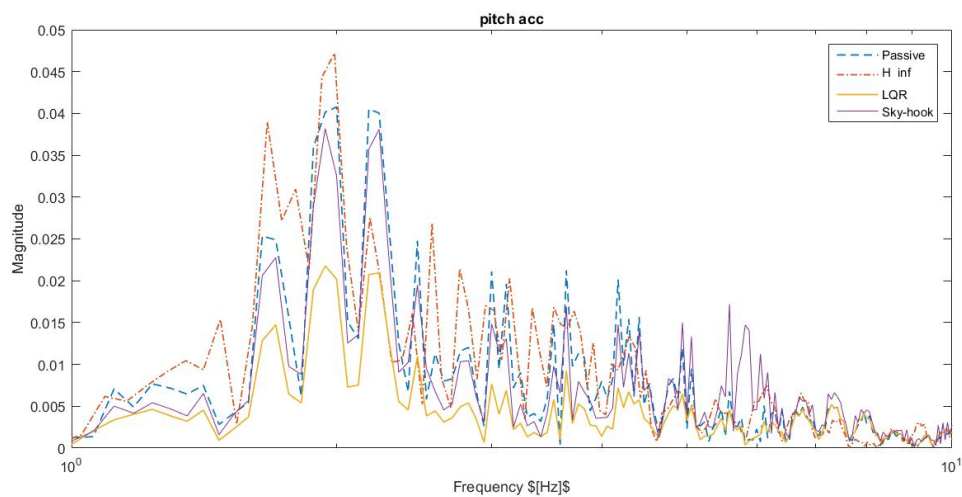

Figure 5.26: Pitch acceleration FFT analysis for the unsymmetrical waves test case

The analysis of pitch acceleration frequency content with FFT method can be seen in figure 5.26. In case of LQR controller, magnitude is decreased along the curves, which means improved ride comfort. Instead, $\mathcal{H}_\infty$ controller achieves worse performance compared to the passive suspension, the signal energy is increased. Sky-hook controller has a slight magnitude decrease than the passive.
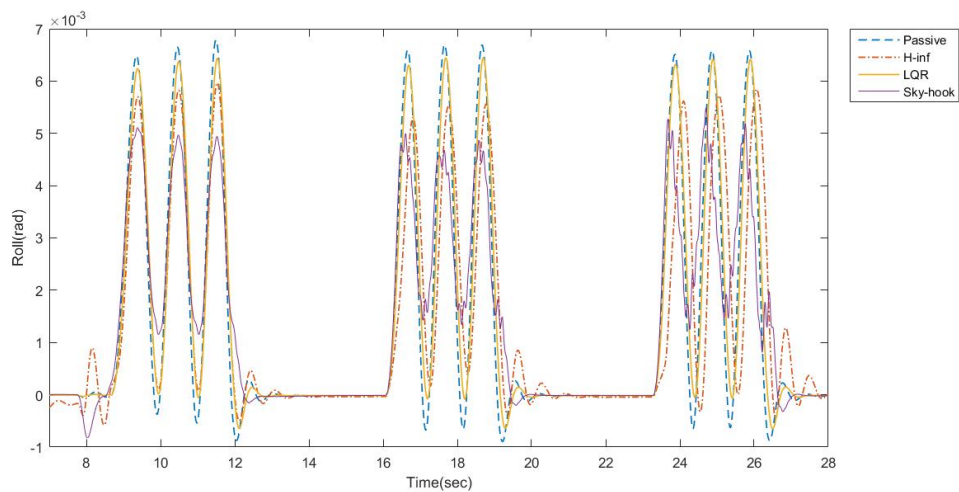
Figure 5.27: Roll angle response for the unsymmetrical waves test case
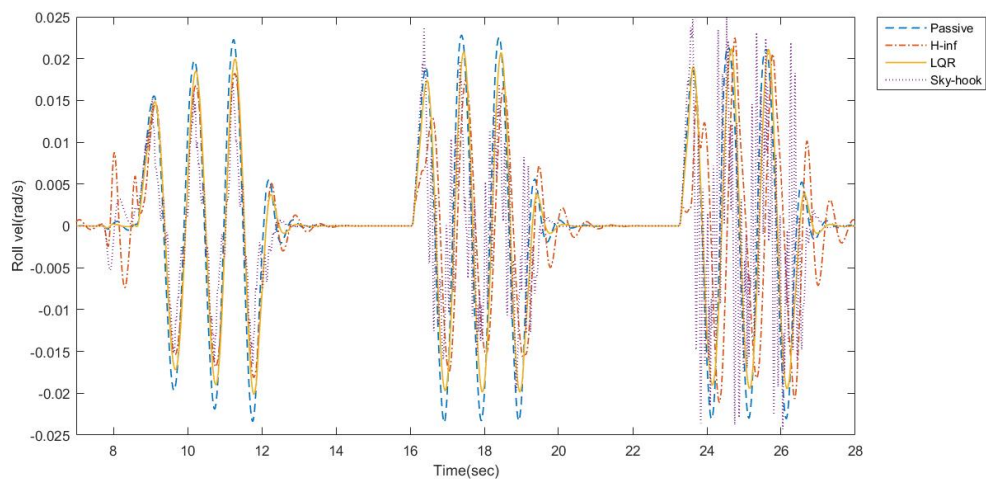

Figure 5.28: Roll velocity for the unsymmetrical waves test case

When the vehicle hits the unsymmetrical waves, roll angle and roll velocity responses can be seen in figure 5.27 and 5.28. Decay rate is faster for the LQR controller. Although in roll velocity the $\mathcal{H}_\infty$ controller has a higher decay rate than the passive system, it has decreased the signals magnitude more than other controllers.
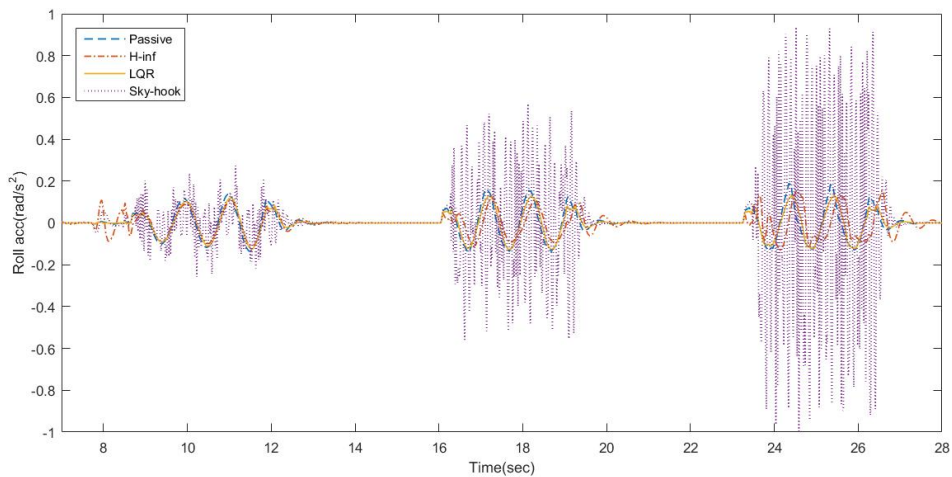
Figure 5.29: Roll acceleration for the unsymmetrical waves test case

Roll acceleration is shown in figure 5.29.

$\mathcal{H}_\infty$ controller has lower peaks compared to the passive, but is reacts slow when it comes to disturbances and it faces difficulties to damp out the resulting oscillations. Sky-hook does not show promising results at all. It can be seen that there are a lot of roll accelerations irregularities and the magnitudes of the curve peaks are much larger those of the passive system, especially when it comes to the waves with larger heights.

However, the LQR controller shows better results. It has a good tracking and the response has been improved. There is no overshoot through the roll acceleration response after waves disturbances.
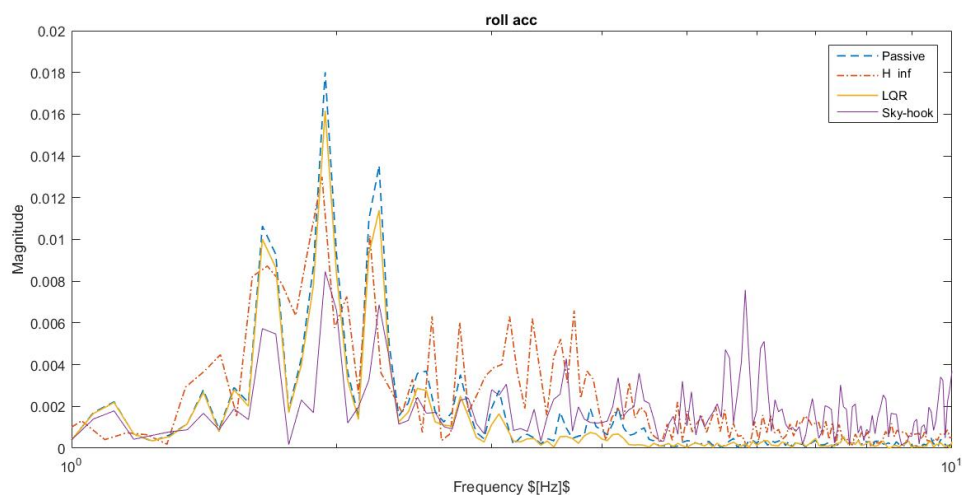

Figure 5.30: Roll acceleration FFT analysis for the unsymmetrical waves test case

Frequency content of roll acceleration can be seen in figure 5.30. The LQR controller produces the same response as passive system. Anyway, the peak values are decreased which results in improved ride comfort in LQR controller. With the $\mathcal{H}_\infty$

controller, the frequency content is increased for more than $2Hz$ but there can be seen decrease on the main peaks. The sky-hook controller, based on results, creates larger frequencies generally that causes vibrations in driving, not a desirable result for the ride comfort.

5.1.4 FEC Track

This test case aims to test the controllers performance in presence of a real road track. This specific road scenario includes bumps and holes with different frequency content. Also the road has negative slope and a turn by the end of the track. The vehicle runs with 50 constant longitudinal speed.
The RMS error are presented in Table 5.7

Table 5.7: RMS errors during FEC track

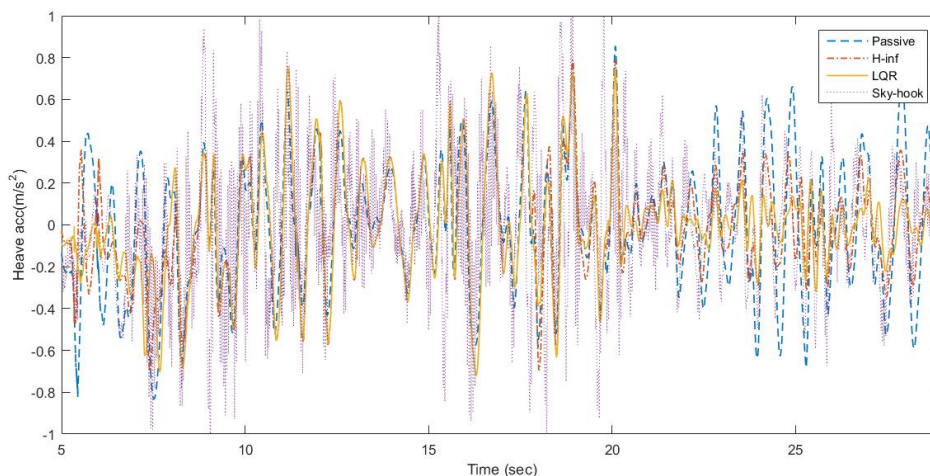| Parameter	Sky-hook	LQR	$\mathcal{H}_\infty$
Heave	0.16%	0.69%	-2.86%
Heave vel	0.12%	0.27%	3.68%
Heave acc	-1.48%	19.1%	12.78 %
Pitch	8.2 %	18.21%	21.76%
Pitch vel	-18.85%	20.41%	0.02%
Pitch acc	-58.42%	17.64%	-0.61%
Roll	-5.69%	-1.25%	20.92%
Roll vel	0%	87.7%	57.36%
Roll acc	-8285%	32.5%	-447.18%

Figure 5.31: Heave acceleration for the FEC track

Figure 5.31 shows heave accelerations of different systems.
For the sky-hook controller, although the RMS value is close to that of the passive system, the sensed heave acceleration is not minimized to improve ride comfort. Based on sky-hook control algorithm, the multiplication sign of deflection velocity

and quarter car body velocity change repetitively through this track, hence the controller reacts to this changes by applying different controller forces to the active damper. Forces are bounded between maximum and minimum amount and they have values with large differences. As a result, the heave acceleration response will oscillate a lot during the road disturbances.

Instead in the LQR controller, fast response to the road disturbances, including negative road slope and vertical accelerations, can be seen. During the last 10 seconds of simulation the oscillations are reduced significantly. The response is smoother than the $\mathcal{H}_\infty$ controller.

In the $\mathcal{H}_\infty$ controller, good tracking of the road can be seen. The RMS error has been improved. During this road profile it decreases the heave acceleration compared the the passive system, same as the LQR controller. The $\mathcal{H}_\infty$ controller has slower response compared to the LQR controller.
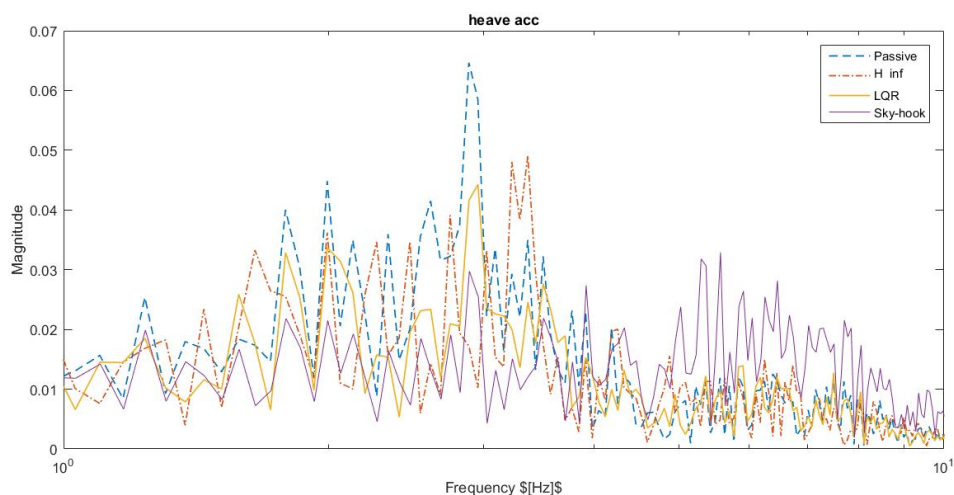

Figure 5.32: Heave acceleration FFT analysis for FEC track

In figure 5.32 heave acceleration FFT analysis can be seen.

LQR controller has decreased the energy which results in better ride comfort compared to the passive system. The $\mathcal{H}_\infty$ controller has shifted to higher frequencies which is desirable for ride comfort and frequency magnitude has been improved too. The sky-hook controller shows increase in magnitude for higher frequencies.
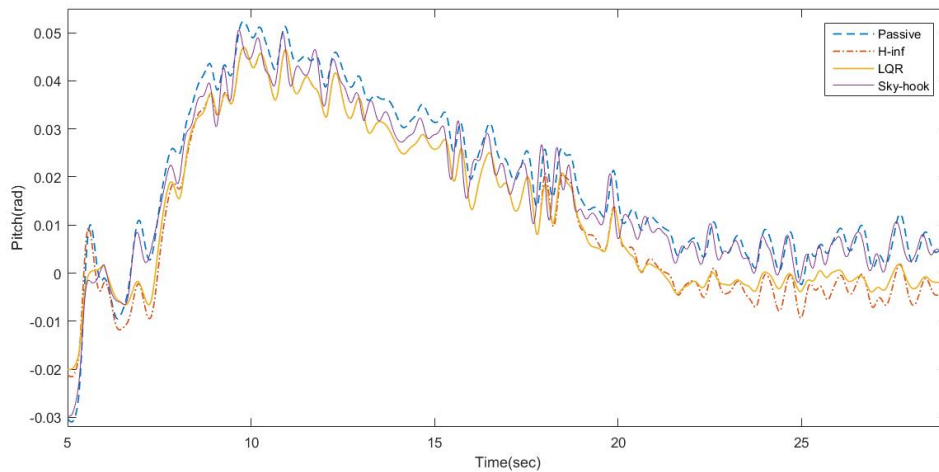
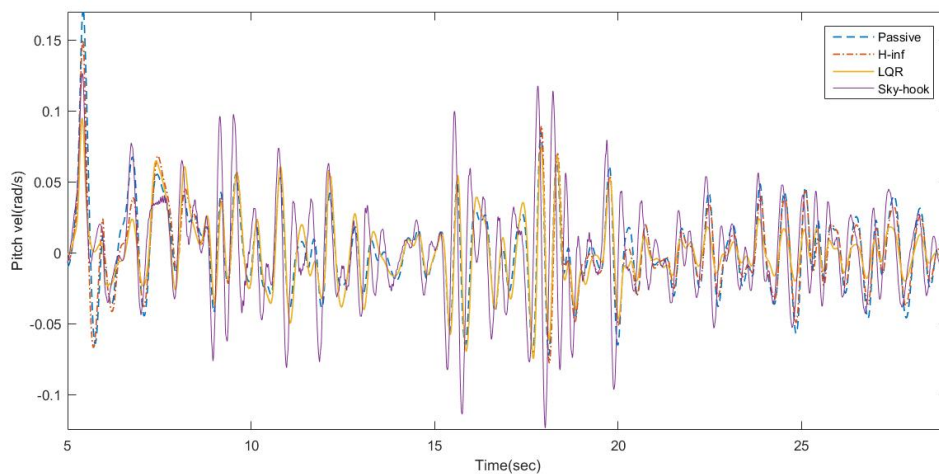**Figure 5.33:** Pitch angle response for the FEC track

Figure 5.34: Pitch velocity response for the FEC track

Pitch angle response is shown in figure 5.33. LQR controller and $\mathcal{H}_\infty$ controller lower the pitch angle and show smoother results compared to the passive suspension. Sky-hook controller does not improve the pitch angle.

Pitch velocity is presented in figure 5.34. Pitch velocity is not improved in $\mathcal{H}_\infty$ controller based on RMS value. LQR has improved the pitch velocity. But the sky-hook controller has increased the pitch velocity.
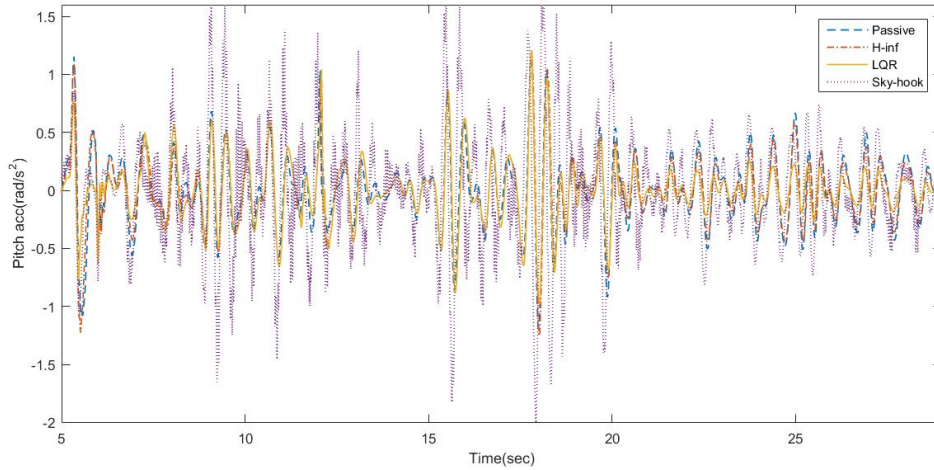
Figure 5.35: Pitch acceleration response for the FEC track

The pitch acceleration in figure 5.35 is shown. For the $\mathcal{H}_\infty$ controller, based on RMS error, there is no improvement and the controller tracks the passive response in this case. LQR controller makes the best improvement compared to the three other systems and shows a fast response. The sky-hook controller does not improve the acceleration, which is not desirable in terms of ride comfort.
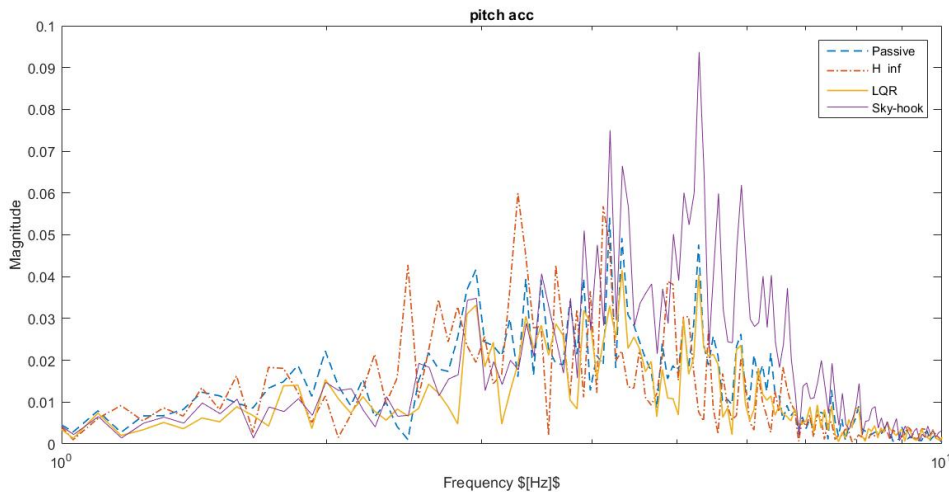

Figure 5.36: Pitch acceleration FFT analysis for the FEC track

LQR controller has lowered the magnitude which results in energy reduction and better ride comfort compared to the passive system. The $\mathcal{H}_\infty$ controller shows mostly decrease in magnitude. The sky-hook controller has increased the energy and shifted it to higher frequencies.
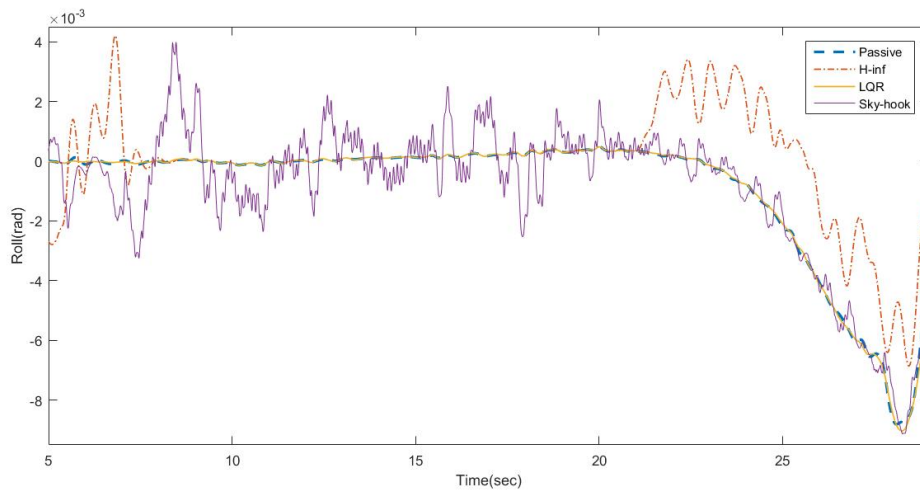
Figure 5.37: Roll angle response for the FEC track

It can be seen in figure 5.37 that the $\mathcal{H}_\infty$ controller is reacting slow the road condition changes which in this test case are the negative slope in the beginning of the track and turn at the end of the track. However the $\mathcal{H}_\infty$ controller shows a good tracking through the track. Roll angle oscillates a lot for the sky-hook suspension system, so it produces a lot of oscillations of the vehicle. The LQR controller shows the best tracking compared to the other systems and smoother results in terms of roll angle.

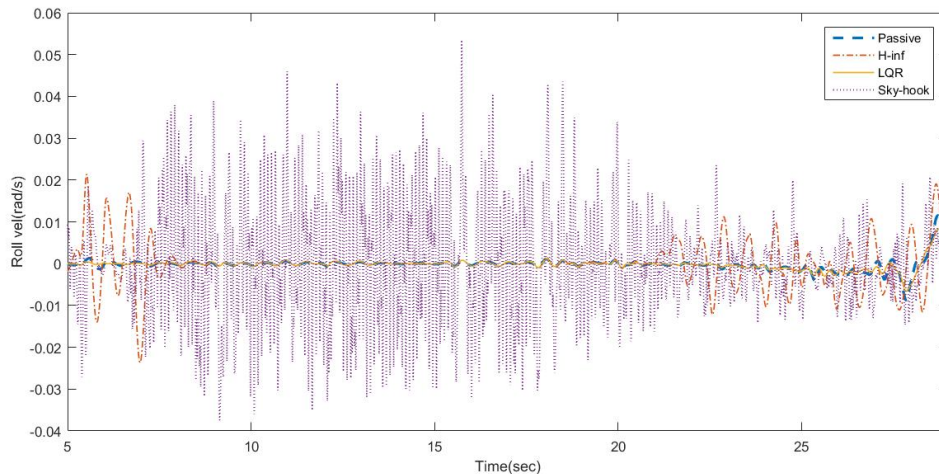**Figure 5.38:** Roll velocity response for the FEC track

It can be seen that the roll velocity has major improvements in the LQR controller and the $\mathcal{H}_\infty$ controller. The $\mathcal{H}_\infty$ controller shows slower response to road conditions. The sky-hook controller has totally failed to mitigate the disturbances of roll velocity compared to the conventional suspension system.
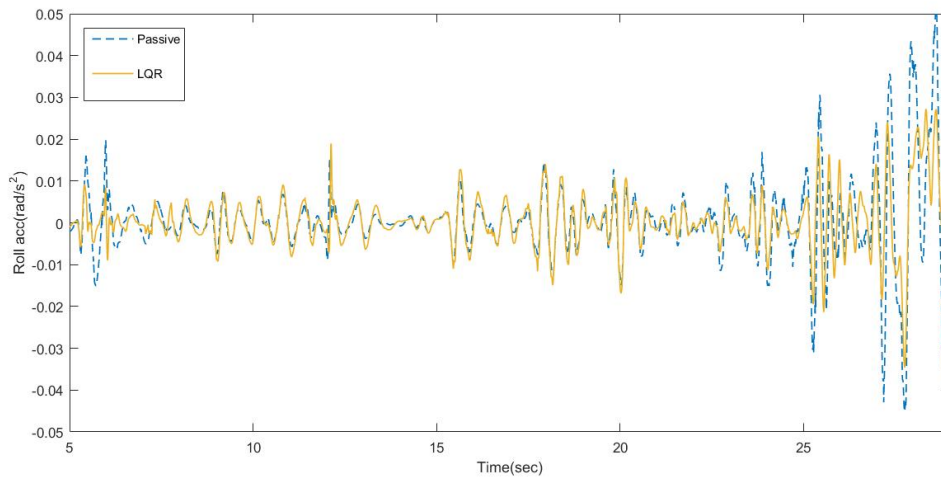
Figure 5.39: Roll acceleration for the FEC track in the passive suspension and the active suspension system equipped with the LQR controller

In roll acceleration analysis, the sky-hook controller a very poor performance which is not acceptable for ride comfort.
figure 5.39 shows a comparison of the roll acceleration for the FEC track between the passive suspension system and the active suspension system equipped with the LQR controller. Based on RMS values, the LQR controller improves the roll acceleration oscillations and shows better responses in larger roll acceleration disturbances compared to smaller ones.
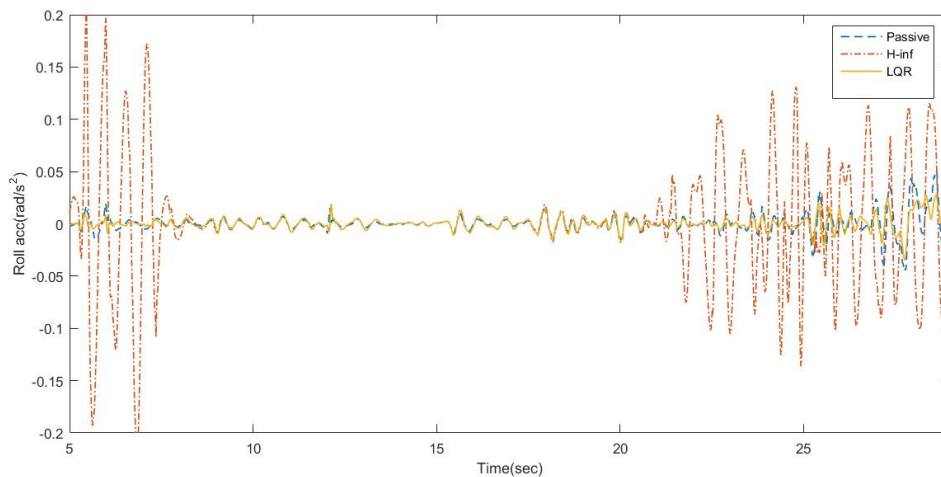
Figure 5.40: Roll acceleration for the FEC track in the passive suspension and the active suspension equipped with the LQR controller and the $\mathcal{H}_\infty$ controller

figure 5.40 shows a comparison of the roll acceleration for the FEC track between the passive suspension system and the active suspension systems equipped with the LQR controller and the $\mathcal{H}_\infty$ controller. The $\mathcal{H}_\infty$ controller show a good trajectory but it reacts slow to the system disturbances. The $\mathcal{H}_\infty$ controller needs to have faster responses and as a result further tuning and system identification are required.

Figure 5.41: Roll acceleration FFT analysis for the FEC track

The $\mathcal{H}_\infty$ controller and the sky-hook controller have increased the signal energy which is not desirable for ride comfort. The LQR controller decreases the magnitude values and shows better results compared to the passive system.

6
Discussion

6.1 System Modelling Analysis

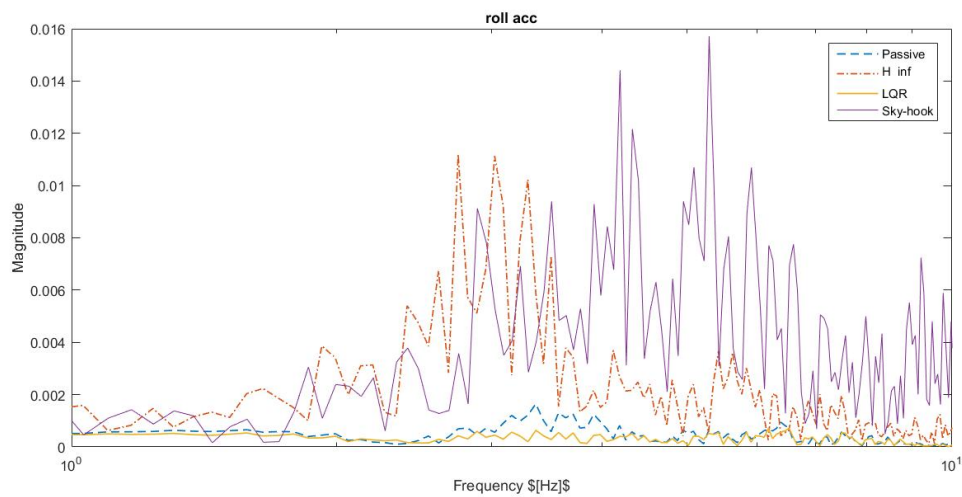The objective of the thesis was to find a suitable controller for controlling the active suspension system in the vehicle.It was required for the analytical dynamics model in MATLAB to achieve a high accuracy compared to the realistic vehicle model in IPG CarMaker. In the analytical full car model, tires were modeled by a spring-damper parallel system. The related damping and stiffness coefficients were tuned in order to calibrate the analytical model from MATLAB on the result from the realistic model from IPG CarMaker. To improve the analytical model fidelity, a more sophisticated tire model can be used.

The active damper model was implemented as a black box in the control system, this applied limitations on the suspension system. In this case, the active damper limited the control forces generated by the control systems. It can be beneficial to investigate more on the different aspects of the active damper system in order to be able to consider more specifications of these active dampers. Hence, for result improvement, it is necessary to do system identification in order to find out more about the active damper behaviour. Based on the results from active damper system identification, control allocations for controllers can be carried out to further adapt the controllers to the active actuators.

6.2 Control System Analysis

The three controllers were tuned to improve ride comfort as target. This tuning may affect the vehicle handling performance. Weighting factors in the controllers designs can be tuned so that the vehicle can perform better in both ride and handling.

Sky-hook control system did not perform well compared to the other systems; even it showed negative RMS errors values in real road track compared to the passive system. This controller is not a fully active control system to control the active forces. The system is bounded and it continuously changes the control forces between maximum and minimum of force values. The body velocity and the deflection velocity in each quarter of the car are changing continuously while running the vehicle. So it is challenging for the sky-hook to command the desired control forces to the suspension system. It can be concluded that sky-hook is not a reliable control system.

The LQR control system is the best active system of the three control system. The RMS errors were positive compared to the passive suspension. In the FFT analysis,

the energy was decreased compared to the other systems.

The $\mathcal{H}_\infty$ showed improved results in ride comfort target. Although, the $\mathcal{H}_\infty$ was expected to show better results than the LQR. By tuning the $\mathcal{H}_\infty$ control system and carrying out further system identifications, it will show better ride comfort results compared to the LQR.

6.3 Future Work

The control parameters in the LQR controller and the $\mathcal{H}_\infty$ controller can be tuned to perform better in terms of the control objectives. Especially the $\mathcal{H}_\infty$ controller has more capabilities and is able to include frequency dependent weights, system uncertainties and limitations on multiple actuators.

Further studies of the system can help to design controllers with better performance. In this regard, frequency analysis of road disturbance can be studied in order to investigate the motion of the vehicle and suspension system. Ride comfort is associated with body accelerations. The suspension travel is constrained by active damper limitations due to damper length. The responses of the open-loop frequency analysis from road inputs and active damper forces to output states can be studied to find out more about the system characteristics. Frequency analysis of active damper can be taken into account.

In $\mathcal{H}_\infty$ control design, uncertainties of suspension components can be included in control actions. Physical uncertainties, deviations of masses and spring stiffnesses can be modelled as physical uncertainties. Also, uncertainties of the active dampers can be included in design specifications.

There are two important targets to improve vehicle dynamics performance: ride target and handling target. Lateral and longitudinal accelerations of the car body can be added to the dynamic model in the control systems for handling performance evaluation. The closed-loop specifications of the ride target and handling target can be considered and controllers can be designed based on those specifications to improve overall performance. This is basically to find a trade-off for controllers to performs well in both ride comfort and handling.

A more realistic tire model and active actuator model can be provided for design improvement. The system delays and computational errors can be analyzed for further development. Energy consumption of the active suspension system can be taken into account in order to optimize the power demand of the vehicle, which has become a hot topic foe the automotive industry.

7
Conclusion

In this thesis full car model was used to simulate the ride comfort. Such full car model represents 7 DOF of the car system, including vertical body motion, pitch, roll and the four tires vertical motions. The vehicle is exposed to unmeasured road profile for controllers to deal with. The active damper systems were limited to force constraints and damper length.

To find a suitable control force for the active suspension system, three different controllers were developed. First, sky-hook controller was implemented. Deflection velocities on all four quarters were used to obtain the desired forces for active damping. Secondly, LQR controller was designed with acceleration penalties and high pass filters for heave, pitch and roll together with the velocity penalties. Finally the third controller was $\mathcal{H}_\infty$ controller with frequency dependant weightings for control effort and error performance penalization. A more detailed model with system specifications was used in the $\mathcal{H}_\infty$ control system. Suspension deflections were penalized, as well as the rates and accelerations of heave, roll and pitch.

The controllers were tested in a realistic simulation environment. Then they were tuned based on relevant scenarios and the tunings procedures kept between different test cases in order to find the most suitable weight sets for each controller .They made improvements of the control objectives and ride comfort performance was improved in most cases. All the controllers showed faster transient response and smoother tracking compared to the passive system.

Sky-hook did not show a promising result in real road track due to simplicity of control policy and limited control actions. In this project, LQR showed the best results in terms of ride comfort control objectives. The $\mathcal{H}_\infty$ control system improved the control objectives and it was expected to show the best ride comfort improvements among other systems. However, based on $\mathcal{H}_\infty$ control potentials, by spending more effort on tuning the control parameters and analyzing the weighting blocks, more improvements can be seen. There is the possibility study more the active dampers more and tune better the related parameters in $\mathcal{H}_\infty$ control.

Hence, for industry use, fully active control systems are required to feed the active suspension system with the desired forces. The $\mathcal{H}_\infty$ and the LQR control systems can be concluded as suitable control solutions for this active suspension system.

To sum up, the controller designs improved the ride comfort; so, the conclusion is in line with thesis objective.

Bibliography

[1] G. Salvendy, *HANDBOOK OF HUMAN FACTORS AND ERGONOMICS*, John Wiley & Sons, Inc. , 2012, ISBN: 978-0-470-52838-9. [online]. `https://kuliahdianmardi.files.wordpress.com/2016/03/handbook-of-human-factors-and-ergonomics-fourth-edition-2012.pdf` Accessed on: 30/01/2019.

[2] B. Heißing and M. Ersoy. *Chassis handbook: fundamentals, driving dynamics, components, mechatronics, perspectives.* Springer Science and Business Media, 2010.

[3] I. Karen, N. Kaya, F. Öztürk, I. Korkmaz, M. Yıldızhan, and A. Yurttas. "A design tool to evaluate the vehicle ride comfort characteristics: modeling, physical testing, and analysis". *The International Journal of Advanced Manufacturing Technology*, vol. 60, pp. 755–763, 2012, `DOI:https://doi.org/10.1007/s00170-011-3592-z`.

[4] Robust Control of an Active Suspension | MathWorks., [Online]. Avalible: `https://se.mathworks.com/help/robust/examples/robust-control-of-an-active-suspension.html`. Accessed on: 30/02/2019.

[5] E. Guglielmino, T. Sireteanu, C. W. Stammers, G. Ghita, and M. Giuclea. *Semi-active suspension control: improved vehicle ride and road friendliness.* Springer Science and Business Media, 2008.

[6] M. Grimstad and F. Zeidler, "Design of MIMO control systems for semi-active dampers combined with active anti-roll bars," M.S. Thesis, Department of Elect. Eng., Chalmers Univ. of Tech., Gothenburg, 2018, [Online]. Available: `http://publications.lib.chalmers.se/records/fulltext/255280/255280.pdf`, Accessed on: 30/05/2019.

[7] H. Agrawal and J. Gustafsson, "Investigation of active anti-roll bars and development of control algorithm," M.S. Thesis, Department of Appl. Mech., Chalmers Univ. of Tech., Gothenburg, 2017, [Online]. Available: `https://pdfs.semanticscholar.org/c310/a3c30270c5240cdc2d6ea9bf47d0ccae30f3.pdf`, Accessed on: 30/05/2019.

[8] F. Kjellberg and S. Sundell, "Real-Time Nonlinear Model Predictive Control for Semi-Active Suspension with Road Preview," M.S. Thesis, Department of Elect. Eng., Chalmers Univ. of Tech., Gothenburg, 2018, [Online]. Available: `https://pdfs.semanticscholar.org/b9de/2277a4c96c55516aa077337bb1ed7c2cedad.pdf`, Accessed on: 30/05/2019.

[9] A. Kruczek, A. Stříbrský, J. Honců, and M. Hlinovský. "Controller choice for car active suspension". *INTERNATIONAL JOURNAL OF MECHANICS*, vol. 3, 2009, [Online]. Avalible: `http://www.naun.org/main/NAUN/mechanics/19-376.pdf`. Accessed on: 30/02/2019.

[10] Carmaker | ipg automotive., [Online]. Avalible: `https://ipg-automotive.com/products-services/simulation-software/carmaker/`. Accessed on: 30/05/2019.

[11] V. Berbyuk, *Vibration Dynamics and control*

[12] Postlethwaite and Ian, *Multivariable Feedback Control: Analysis and Design*, John Wiley & Sons, Inc. , 1996, ISBN: 0471943304.

[13] B. Kulscar, Class Lecture, Topic: " Linear Control System Design." SSY285, Department of Electrical Engineering, Chalmers University of Technology, Gothenburg, 2017.

[14] B. Kulscar, Class Lecture, Topic: " Robust and Nonlinear Control." ESS076, Department of Electrical Engineering, Chalmers University of Technology, Gothenburg, 2018.

[15] Gu, D.W. and Petkov, P. and Konstantinov, M.M., *Robust Control Design with MATLAB®*, ser. Advanced Textbooks in Control and Signal Processing, Springer London, 2005, ISBN: 9781852339838.

[16] Petter Lundström, Sigurd Skogestad, Zi-Qin Wang, "Performance weight selection for $\mathcal{H}_\infty$ and μ control methods," *Transactions of the Institute of Measurement and Control*, vol. 13, no. 5, pp. 241–252. DOI:https://doi.org/10.1177/014233129101300504

[17] Bibel, J.E. and Malyevac, D.S. and NAVAL SURFACE WARFARE CENTER DAHLGREN DIV VA., *Guidelines for the Selection of Weighting Functions for $\mathcal{H}_\infty$ Control*, Defense Technical Information Center, 1992.

[18] "First and second order filters," [Online]. Available: http://www.doe.carleton.ca/~rmason/Teaching/486-d.pdf., Accessed on: 30/05/2019.

[19] Max Kamenetsky, "Filtered audio demo," [Online]. Available: https://web.stanford.edu/~boyd/ee102/conv_demo.ps, Accessed on: 30/05/2019.

[20] Jazar, R.N., *Vehicle Dynamics: Theory and Application*, Springer International Publishing, 2017, ISBN: 9783319534411.

[21] Rajesh Rajamani, *Vehicle Dynamics and Control*, Springer International Publishing, 2006, ISBN: 9780387263960.

[22] Statista., [online]. https://www.statista.com/forecasts/997119/purchase-criteria-for-cars-in-the-us Accessed on: 30/01/2019.

[23] Frisk, D. (2016) A Chalmers University of Technology Master's thesis template for LaTeX. Unpublished.